minerals

MDPI

Article

Bentonite Alteration in Batch Reactor Experiments with and without Organic Supplements: Implications for the Disposal of Radioactive Waste

Carolin Podlech [1,*], Nicole Matschiavelli [2], Markus Peltz [1], Sindy Kluge [2], Thuro Arnold [2], Andrea Cherkouk [2], Artur Meleshyn [3], Georg Grathoff [1] and Laurence N. Warr [1]

[1] Institute of Geography and Geology, University of Greifswald, 17489 Greifswald, Germany; markus.peltz@uni-greifswald.de (M.P.); grathoff@uni-greifswald.de (G.G.); warr@uni-greifswald.de (L.N.W.)
[2] Institute of Resource Ecology, Helmholtz-Zentrum Dresden-Rossendorf, 01328 Dresden, Germany; n.matschiavelli@hzdr.de (N.M.); s.kluge@hzdr.de (S.K.); t.arnold@hzdr.de (T.A.); a.cherkouk@hzdr.de (A.C.)
[3] Gesellschaft für Anlagen- und Reaktorsicherheit (GRS) gGmbH, 38122 Braunschweig, Germany; artur.meleshyn@grs.de
* Correspondence: carolin.podlech@uni-greifswald.de

Abstract: Bentonite is currently proposed as a potential backfill material for sealing high-level radioactive waste in underground repositories due to its low hydraulic conductivity, self-sealing ability and high adsorption capability. However, saline pore waters, high temperatures and the influence of microbes may cause mineralogical changes and affect the long-term performance of the bentonite barrier system. In this study, long-term static batch experiments were carried out at 25 °C and 90 °C for one and two years using two different industrial bentonites (SD80 from Greece, B36 from Slovakia) and two types of aqueous solutions, which simulated (a) Opalinus clay pore water with a salinity of 19 g·L^{-1}, and (b) diluted cap rock solution with a salinity of 155 g·L^{-1}. The bentonites were prepared with and without organic substrates to study the microbial community and their potential influence on bentonite mineralogy. Smectite alteration was dominated by metal ion substitutions, changes in layer charge and delamination during water–clay interaction. The degree of smectite alteration and changes in the microbial diversity depended largely on the respective bentonite and the experimental conditions. Thus, the low charged SD80 with 17% tetrahedral charge showed nearly no structural change in either of the aqueous solutions, whereas B36 as a medium charged smectite with 56% tetrahedral charge became more beidellitic with increasing temperature when reacted in the diluted cap rock solution. Based on these experiments, the alteration of the smectite is mainly attributed to the nature of the bentonite, pore water chemistry and temperature. A significant microbial influence on the here analyzed parameters was not observed within the two years of experimentation. However, as the detected genera are known to potentially influence geochemical processes, microbial-driven alteration occurring over longer time periods cannot be ruled out if organic nutrients are available at appropriate concentrations.

Keywords: bentonite; smectite; layer charge; metal substitution; SEM–EDS; microbial diversity; organic supplements

Citation: Podlech, C.; Matschiavelli, N.; Peltz, M.; Kluge, S.; Arnold, T.; Cherkouk, A.; Meleshyn, A.; Grathoff, G.; Warr, L.N. Bentonite Alteration in Batch Reactor Experiments with and without Organic Supplements: Implications for the Disposal of Radioactive Waste. *Minerals* **2021**, *11*, 932. https://doi.org/10.3390/min11090932

Academic Editors: Ana María Fernández, Stephan Kaufhold, Markus Olin, Lian-Ge Zheng, Paul Wersin and James Wilson

Received: 24 June 2021
Accepted: 20 August 2021
Published: 27 August 2021

1. Introduction

Bentonite clay is a natural material consisting predominantly of dioctahedral smectites, mainly montmorillonite of the montmorillonite-beidellite series [1,2]. Due to its very low hydraulic conductivity, high swelling capability and strong buffering capacity when hydrated, the material is considered to be ideal for sealing the underground repository space between canisters containing high-level radioactive waste (HLW) and the host rock formation [3,4]. Despite the versatility of this material, questions remain on the long-term stability of the bentonite in a repository setting, in particular when subjected to conditions of chemical disequilibrium caused by the circulation of formational ground waters

and/or when in contact with corrodible metal canisters [5,6] or supporting cementitious materials [7,8]. Only if repositories remain intact for up to one million years, as foreseen in Germany [4], will any leakage of residual radioactive substances into biosphere be prevented.

The chemical stability of smectite is important when it comes to the longevity of the bentonite barrier. A key process for mineral transformation is the smectite-to-illite conversion, whereby the needed K^+ cations may be supplied by dissolved accessory minerals or formation groundwater [9]. Thus, the stability of smectite in contact with salt solutions has been the topic of numerous studies that considered variations in pH, salinity and/or temperature conditions [10–12].

An additional aspect of the bentonites long-term stability is the potential influence of microbial activity in environments within the repository setting. Whereas it is generally accepted that such activity will not be of importance in highly compacted bentonite materials (dry density $\geq$ 1600 kg·m^{-3}) [13], where the tight pore space and very low hydraulic conductivities will limit transport and mobility, there will be niches in the repository site where erosion and particle transport could lead to less compacted material and the development of bentonite clay slurries [14].

Microbial activity has been shown to affect the properties of smectitic clay minerals as well as the adsorption of metals and actinides by a number of processes, including the mobilization and immobilization of toxic elements and radionuclides [15,16]. It is also known that the presence of sulfate-reducing bacteria (SRB) can lead to the formation of hydrogen sulfides (H_2S) and promote corrosion of metals [17,18]. As a result, Fe^{3+} is reduced to Fe^{2+} [19], whereby the metal Fe can destabilize dioctahedral smectites by Fe^{2+} migration into the interlayer [20] and thus influence the smectites adsorption behavior, relevant to metal and radionuclides retardation [21].

The main objective in this study was to determine the alteration mechanisms of bentonites influenced by temperature, solution chemistry and microbial diversity using energy dispersive X-ray (EDX) spectroscopy analyses of extracted and purified smectite fractions as the primary method. For this purpose, we analyzed two sets of bentonite samples (SD80, B36) that differ in their mineralogical and chemical properties (i.e., accessory content, Fe content in smectite and layer charge distribution).

The series of slurry bentonites prepared with and without microbial substrates that were experimentally investigated reveal that minor but permanent changes in the smectite composition did occur that are attributable to the tetrahedral substitution of Si^{4+} by Al^{3+} and more variable octahedral substitution between Fe^{3+}, Mg^{2+} and Al^{3+}. Our findings also emphasize that the microbial diversity depended on the bentonite itself as well as the applied conditions. However, there is no evidence that the observed smectite alterations were induced by microbial activity. Such alterations are more likely influenced by the addition of organic substrates, which are known to act as electron-donors and promote protonation/deprotonation surface reactions.

2. Materials and Methods

2.1. Experimental Set-Up

For the batch-experiments, two uncompacted European Ca-bentonites (SD80 from Milos, Greece and B36 from Lieskovec, Slovakia) were used. In order to obtain representative samples, both bentonites were mechanically homogenized prior to the experiments. Both bentonite samples were kindly provided by Stephan Kaufhold (BGR Hannover), whereby the B36 bentonite has been extensively characterized in previous studies [22,23].

Long-term batch experiments were performed at the "Gesellschaft für Anlagen-und Reaktorsicherheit" (GRS, Braunschweig) using two temperatures and two types of solution, which were prepared under ambient atmosphere (Figure 1, Table S1). Bentonites were reacted in sealed glass vessels (flushed with argon 4.6, 99.996% purity, 2–3 min) with either a synthetic Opalinus clay pore water (OPA) [24] with a salinity of 19 g·L^{-1} or a diluted cap rock solution (CAP) [25] with a salinity of 155 g·L^{-1}. The solid to solution ratio by weight

was set at 1:2. The bentonite slurries were exposed to two different temperatures (25 °C and 90 °C) for periods of one and two years without compaction or shaking. To study microbial diversity, batches supplemented with organic substrate (+S) were compared to control batches without organic substrate (–S). The substrate-mix was comprised of 0.05 mol·L^{-1} sodium lactate, 0.05 mol·L^{-1} sodium acetate, 0.003 mol·L^{-1} methanol and 0.0001 mol·L^{-1} anthraquione-2,6-disulfonate (AQDS) to stimulate the indigenous, viable microbial community. The complete experimental setup, including gases, substrates, pore waters and bentonites, was not assembled under sterile conditions. However, the amount of microbial contamination in previous studies using the same setup prepared under sterile conditions was shown to be not significant [26].

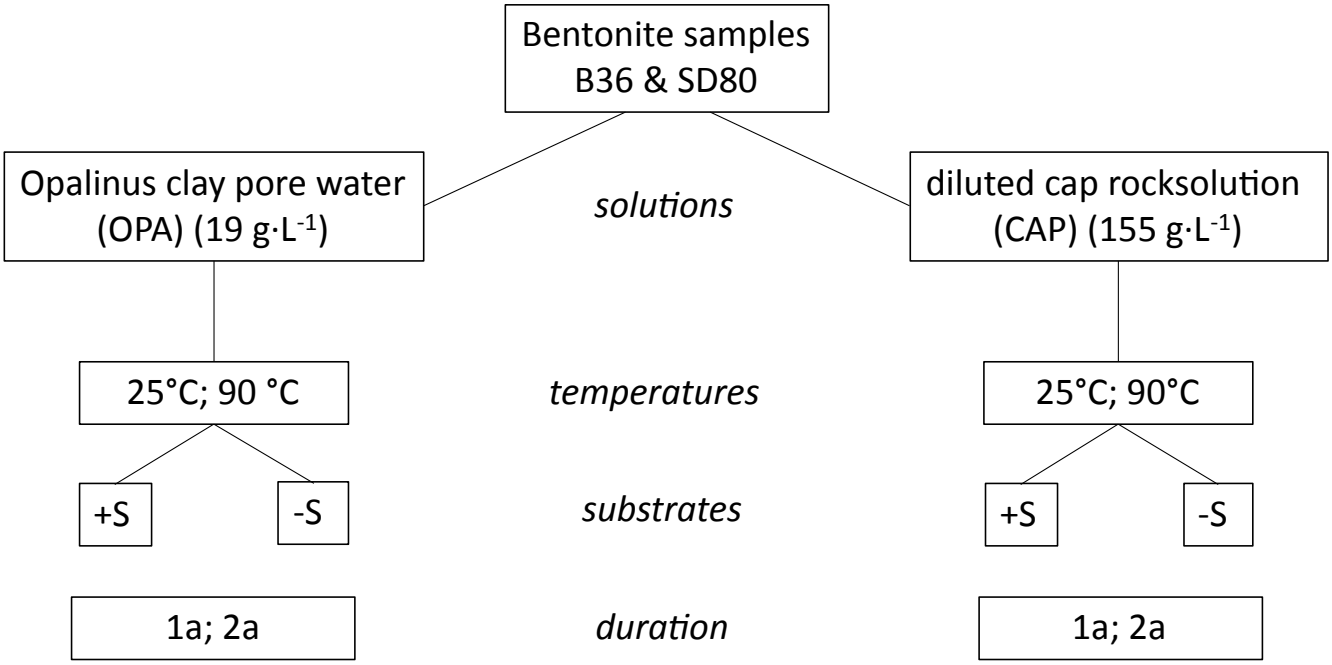

Figure 1. Flowchart illustrating the general setup of the bentonite batch-experiments. OPA: synthetic Opalinus clay pore water, CAP: synthetic diluted cap rock solution, +S: with substrate (Na-lactate, Na-acetate, methanol, AQDS), −S: without substrate, 1a: incubation for one year, 2a: incubation for two years.

The sampling of batches was carried out at the GRS laboratories. Bentonite slurries were extracted under sterile conditions for analyzing the microbial diversity. Therefore, up to 50 mL of bentonite suspension was transferred with a sterile spatula into sterile tubes. The respective samples were stored at −70 °C prior to extraction of the DNA. Afterwards, some supernatant solution was filtered and collected for ICP-OES analyses and 5–10 g of bentonite slurry sampled for mineralogical analysis. Subsequently, these samples as well as the raw materials were washed with distilled water using dialysis tubes (Spectra/Por® 1 dialysis membrane with a molecular weight cut-off of 6–8 kD) to remove excess salts such as those introduced by the OPA or CAP solutions. Afterwards, the samples were dried in an oven at 60 °C.

2.2. Bentonite Characterization (XRF, CEC, XRD)

The dialyzed bentonite powder was investigated using the following techniques. The major element oxide composition was analyzed by X-ray fluorescence spectroscopy (XRF) using a Philips PW2404 X-ray spectrometer (Tables S2 and S3). The water content was determined by oven drying an 800 mg bentonite sample at 105 °C until constant weight was achieved after about 7 days followed by heating the sample to 1050 °C for 1 h. The total change expressed as the loss-on-ignition (LOI) was determined based on the differences in

mass. Afterwards, the samples were melted with a flux ($LiBO_2$ + $Li_2B_4O_7$) at 1100 °C to prepare fused tablets. Analytical measurements were calibrated against USGS standards (BHVO-2, AGV-2 and RGM-1).

The cation exchange capacity (CEC) was determined using the Cu(II)-trien method [27,28]. CEC measurements were repeated three times for each sample. The results were used to calculate mean values and standard deviations. Afterwards, the Cu(II)-trien exchanged cations (EC) Na^+, K^+, Ca^{2+} and Mg^{2+} were measured by atomic absorption spectroscopy (AAS).

The mineralogical composition of the bentonites was determined by X-ray diffraction analysis (XRD) using a Bruker D8 Advance θ–θ diffractometer with Fe-filtered CoKα radiation (40 kV, 30 mA). The diffractometer was equipped with a 0.5° divergence slit and a 1D LynxEye detector. Scans were collected between 4° and 80° 2θ for randomly oriented powders (scanning rate 1° 2θ/min) and between 4° and 50° 2θ for preferred oriented samples (scanning rate 3° 2θ/min) with a step size of 0.02° 2θ. The oriented samples were measured in the air-dried (AD) state and after ethylene glycol (EG) saturation. The XRD quantification were carried out with the Rietveld program BGMN and the user-interface Profex 4.0 [29].

2.3. Smectite Characterization (SEM-EDX)

The chemical composition of smectites was studied by scanning electron microscopy (SEM) in combination with EDX spectroscopy. The elemental abundance of purified smectite fractions were quantified as oxides and used to calculate the structural formulae and consequently the layer charge.

For sample purification, 200 mg of bulk material was weighed and placed in centrifuge tubes in 40 mL of deionized water. For initial removal of any remaining salts, the samples were sedimented by high speed centrifugation and the double distilled water replaced. Afterwards, the sample was redispersed using an ultrasonic bath. The smectite separation was performed by repeated centrifugation using an Eppendorf 5810 R centrifuge (800 rpm, 18 min) to separate the <1 µm size fraction. After each centrifugation, the supernatant was transferred to a clean centrifuged tube and topped up with deionized water prior to ultrasonic treatment, and then the centrifugation repeated. This cycle of treatment was repeated 11 times until no impurities were detected by XRD. One drop of the purified smectite suspension was then mounted on a polished pure graphite rod to obtain a homogenous flat layer of smectite particles. Before measurement, the samples were sputtered with palladium (Pd) to minimize charging effects.

SEM–EDX analyses were performed using a Zeiss Auriga scanning electron microscope equipped with an Oxford instruments X-MAX 80 mm^2 EDX silicon drift detector and a field emission cathode. Electron images were taken using a secondary electron (SE2) detector. Smectite elemental chemistry was determined on the basis of EDX mappings at 15 kV and a working distance of 5 mm. Elemental maps of homogenous, flat sample areas were obtained at 6000-fold magnification, a dwell time of 100 µs and by using an automatic drift correction. Thirty frames were collected for each map and three maps were obtained from independent areas of each sample, which were averaged to obtain the smectite composition (Tables S4 and S5). By using this routine, any areas of obvious contamination could be detected and excluded from the quantification. Data acquisition was performed with the software INCA (Oxford instruments) including pulse pile-up, escape peak and ZAF corrections. Oxygen measurements were not used for quantifications, and the results were instead normalized to 100% assuming that all cations were present as oxides.

The elemental mapping approach was used to overcome common problems of EDX analyses as described in detail by Christidis [30]. For quantifications, high precision, accuracy and sample homogeneity are mandatory. To reach appropriate precisions, Williams and Carter [31] suggested using total counts of at least 10^4 above the background for each characteristic peak. This was achieved by using the aforementioned settings, which were further optimized to minimize potential loss of mobile cations such as alkali elements

(e.g., K^+ or Na^+) due to beam damage [32,33], which is particularly evident during point analyses and worsens with measuring time. Although some local migration of cations may still occur during mapping even with short dwell times, it is assumed that the cations do not leave the mapped area of the specimen and that the averaged values remain constant throughout the measurement period.

As no commercially available EDX standards exist that are suitable for smectite calibration, standardless quantifications based on the vendor supplied pure element calibration of the detector were carried out [34]. The elemental-wise accuracy of the measurements was determined by applying the same measurement routine to ASTIMEX silicate standards with similar elemental compositions. The mean absolute deviations from the expected values in wt.% for analyses were 0.04 wt.% between 0 and 1 wt.%, 0.51 wt.% between 1 and 10 wt.% and 0.73 wt.% between 10 and 100 wt.%. Based on all standard measurements, the element specific mean deviations in wt.% were 0.31 for Na (0–5 wt.%), 0.09 for K (0–5 wt.%), 0.33 for Ca (0–5 wt.%), 0.07 for Mg (0–5 wt.%), 0.28 for Al (0–16 wt.%), 0.61 for Si (0–35 wt.%) and 0.46 for Fe (0–10 wt.%).

The chemical composition of the purified smectite samples was used to calculate the structural formula (SF) based on the method of Stevens [35]. The SF calculation was carried out on the basis of 11 oxygen atoms per half unit cell (phuc), where H_2O and F are not considered. For the calculation it was assumed that the tetrahedral sheet consists of 4 atoms (Al + Si), whereas the occupancy of the octahedral sheet is assumed to be fixed with 2 atoms (Al + Fe + Mg). The exchangeable cations Na, K, Ca and excess Mg that cannot be incorporated into an octahedral site were assigned to the interlayer. AAS measurements of exchangeable cations after Cu(II)-trien exchange also confirmed the presence of Mg in the interlayer of both samples (Section 3.1). As the true oxidation state of Fe is unknown, Fe^{3+} was assumed, as it is the dominant form in dioctahedral smectites [36]. Trace amounts of TiO_2 (<1 wt.% XRF) were related to anatase and/or rutile and thus excluded from the structural formula calculations. Based on the accuracy, precision and sample homogeneity of this method, changes of $\geq$0.02 equivalents per half unit cell ($e \cdot phuc^{-1}$) are considered detectable.

2.4. Solution Chemistry (pH, ICP-OES)

The pH measurements of the supernatants were performed at 25 °C after short term experimentation (up to 30 days) in a glove box with argon atmosphere and after long term batch experimentation (after one and two years) in glass vessels. The pH values of both solutions (CAP, OPA) were taken as reference values.

The cation concentrations (Si, Mg, Ca, Na, K) of the solutions before and after experimentation were analyzed using an iCAP 7400 Duo inductively coupled plasma optical emission spectrometer (ICP-OES) (Thermo Fisher Scientific). Fe- and Al contents could not be determined as they were below detection limit. The chloride concentration was determined potentiometrically using the titration system Titrando 857 (Metrohm).

2.5. DNA Extraction, Amplification of 16S rRNA Gene and Sequencing

For analyzing the microbial diversity within the respective samples, DNA extraction and amplification of the V4-region was conducted according to the protocol of Matschiavelli et al. [37] without modifications.

Retrieved 16S rRNA gene sequences are available from the NCBI database with the bioproject accession number PRJNA758205 (https://www.ncbi.nlm.nih.gov/; accessed on 27 August 2021).

3. Results

3.1. Characterization of Starting Material

Both bentonites differed in their chemical and mineralogical composition (Tables 1 and 2). The main components of SD80 are smectite and feldspar, whereby quartz, anatase, calcite, pyrite and baryte occur as traces with <1 wt.% (Figure 2a). Sample B36 mainly consists of

smectite, feldspar and quartz with minor amounts of cristobalite, kaolinite and anatase (Figure 2b). In comparison to SD80, B36 showed higher concentrations of SiO_2 and K_2O, which are associated with larger amounts of accessory minerals (~35 wt.%), i.e., feldspar, quartz and cristobalite. The 060-reflection of the randomly oriented powders were between 0.149 and 0.152 nm (Table 3) and correspond to dioctahedral smectite [38]. The 001-reflection of the oriented slides in air-dried condition (~60% RH) was located around 1.5 nm, which is characteristic of smectite with bivalent interlayer cations (Ca^{2+} and/or Mg^{2+}) hydrated by two water layers [39]. The higher Fe_2O_3 content is related to Fe-rich smectite in B36 (Table 4). These results are similar to those obtained by Ufer et al. [22], who characterized mineralogically (XRD) and geochemically (XRF) various Greek Milos bentonites (cf. SD80) as well as bentonites from Slovakia (cf. B36).

Table 1. XRF main elemental composition of the bulk material (data in oxide wt.%). LOI: loss-on-ignition.

Sample	LOI	SiO_2	Al_2O_3	Fe_2O_3	MgO	CaO	K_2O	TiO_2	Na_2O	MnO	P_2O_5	Sum
SD80	16.5	51.7	17.9	4.8	2.9	2.5	0.9	0.7	0.7	0.1	0.2	99.4
B36	13.9	58.6	16.3	7.4	1.5	1.2	1.5	0.8	0.4	0.1	0.1	101.8

Table 2. XRD quantification results based on Rietveld-Refinement. Ant: anatase, Brt: baryte, Cal: calcite, Crs: cristobalite, Fsp: feldspar, Kln: kaolinite, Sme: smectite, Py: pyrite, Qz: quartz, n.d.: not determined (data in wt.%). IMA-CNMNC approved mineral symbols after Warr [38].

Sample	Sme	Fsp	Qz	Kln	Crs	Ant	Cal	Py	Brt
SD80	89	7	<1	n.d.	n.d.	<1	<1	<1	1
B36	65	15	12	4	4	<1	n.d.	n.d.	n.d.

Table 3. XRD parameter of both bentonites. RP: random powder, AD: air dried, EG: ethylene glycol-saturated, FWHM: full-width-at-half-maximum.

Sample	d_{001} [nm]	d_{060} [nm]	d_{001} [nm]		d_{001} FWHM [Δ° 2θ]	
	RP	RP	AD	EG	AD	EG
SD80	1.52	0.150	1.45	1.68	1.8	0.6
B36	1.50	0.150	1.48	1.68	1.4	0.8

Table 4. Structural formula of purified smectites (<1 μm) based on elemental composition determined by EDX (values are rounded and given in e·phuc^{-1}).

Sample	Tetrahedral Cations		ξ_{tet}	Octahedral Cations			ξ_{oct}	Interlayer Cations				ξ	ξ_{tet}
	Si^{4+}	Al^{3+}		Al^{3+}	Fe^{3+}	Mg^{2+}		Ca^{2+}	Na^{+}	K^{+}	Mg^{2+}		%
SD80	3.94	0.06	−0.06	1.44	0.26	0.30	−0.30	0.09	0.01	0.03	0.06	−0.36	17
B36	3.79	0.21	−0.21	1.37	0.46	0.16	−0.16	0.11	0.01	0.03	0.06	−0.38	56

Based on EDX-derived compositions of purified mineral fractions and by applying the smectite classification scheme of Emmerich et al. [40], the SD80 smectite was classified as a low charged beidellitic montmorillonite with a tetrahedral charge of 17% and a total layer charge of $\xi = -0.36$ e·phuc^{-1} and the smectite of B36 as a medium charged Fe-rich montmorillonitic beidellite with 56% tetrahedral charge and a total layer charge of $\xi = -0.38$ e·phuc^{-1} (Table 4).

The SD80 bentonite, with almost 90 wt.% smectite content, had a higher CEC value of 87 ± 2.2 cmol·kg^{-1} compared to the 54 ± 2.0 cmol·kg^{-1} of the B36 bentonite with 65 wt.% smectite (Table 5). Both bentonite interlayers were dominated by bivalent cations with ≥50% Ca^{2+} and about 30% Mg^{2+}. For SD80, the sum of exchangeable cations was equal to the determined CEC but differed slightly for sample B36, whereby the measured CEC was

higher than the sum of EC. The latter could be an indication of excess adsorption of the Cu-trien index cation on clay mineral edges.

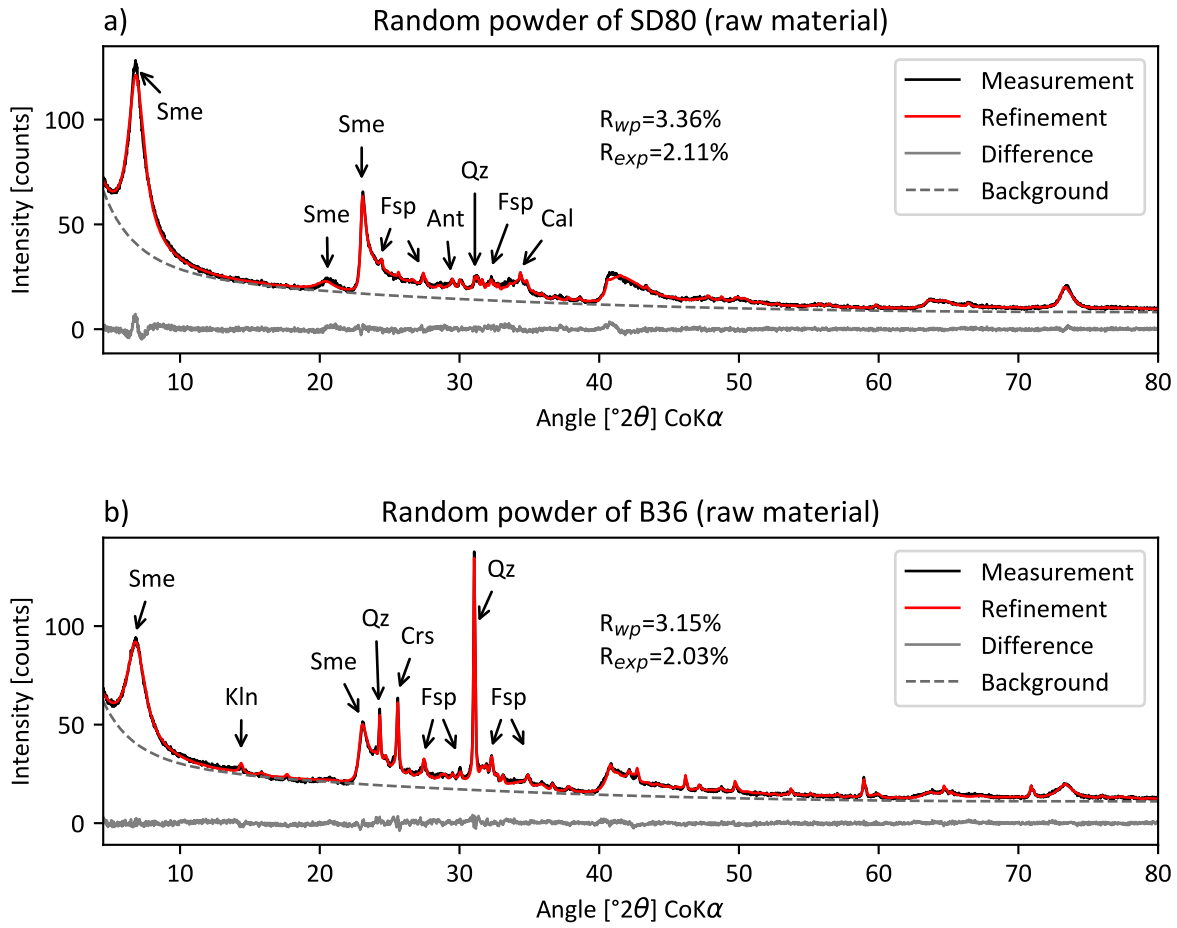

Figure 2. X-ray diffraction pattern of random powders from (**a**) SD80 and (**b**) B36 with Ant: anatase, Cal: calcite, Crs: cristobalite, Fsp: feldspars, Kln: kaolinite, Sme: smectite, Qz: quartz, R_{wp}: weighted residual square sum, R_{exp}: theoretical minimum value for R_{wp}.

Table 5. CEC values and exchangeable cations (EC) of both bentonites after Cu-trien saturation (sample weight 150 mg/60 mL).

Sample	CEC	Na^+	K^+	Ca^{2+}	Mg^{2+}	$\Sigma_{cations}$
	$cmol \cdot kg^{-1}$	$cmol \cdot kg^{-1}$	$cmol \cdot kg^{-1}$	$cmol \cdot kg^{-1}$	$cmol \cdot kg^{-1}$	$cmol \cdot kg^{-1}$
SD80	87 ± 2.2	17 ± 0.4	2 ± 0.06	43 ± 2.4	23 ± 2.3	86 ± 2.6
B36	54 ± 2.0	1 ± 0.03	1 ± 0.04	30 ± 1.4	14 ± 0.4	46 ± 1.8

3.2. Characterization of the Reacted Bentonites

3.2.1. Visual Changes of the Bentonite Batches

After long-term experimentation, the bentonite batches showed distinct color changes. The one-year samples reacted in OPA solution had a blueish coloration (Figure 3a,b), whereas the corresponding two-year batches appeared more beige or greyish (Figure 3c,d). In addition, the B36 samples appeared brownish with a characteristic green coloration at the bentonite–solution interface, which indicates potential Fe-reduction [41] (Figure 3d). Within the substrate-bearing SD80 bentonite, the occurrence of black spots as well as the formation of gas bubbles (Figure 3a) and horizontal fissures due to gas release (Figure 3c) were

observed in some of the reacted samples. The development of layers due to sedimentation is highlighted by a dotted line in the respective samples in Figure 3b–d.

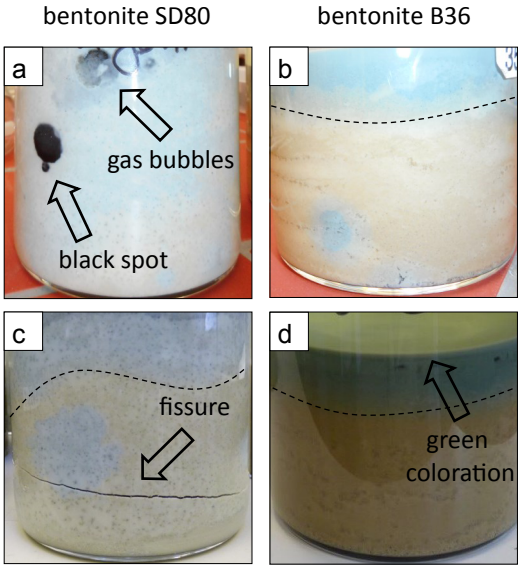

Figure 3. Color changes of both batches (SD80, B36) subjected to Opalinus clay pore water at 25 °C supplemented with substrate. Bentonite SD80 showed (**a**) the occurrence of black spots and gas bubbles after one year and (**c**) a horizontal fissure after two years. Bentonite B36 showed (**b**) a blueish coloration after one year and (**d**) a characteristic green coloration at the bentonite–solution interface after two years.

3.2.2. Microbial Diversity Analysis

In order to investigate a potential microbial effect on the here tested mineralogical parameters of B36 and SD80, the microbial diversity of the respective slurry experiments was analyzed and compared to the respective bentonite raw materials. In general, the concentration of extracted DNA was very low and for most samples almost below the detection limit (Table S6). Successful extraction and sequencing of DNA was achieved for seven samples, including the raw material of SD80 and B36 (Figure 4).

The sequencing results showed that the microbial diversity of the two initial bentonites were different from each other, and that the diversity changed in response to the applied conditions. Supplemented batches that contained SD80 bentonite and that were reacted in OPA solution at 25 °C for one and two years showed the formation of black precipitates and fissures (Figure 3a) as well as the dominance of spore-forming and sulfate-reducing bacteria from the genera *Desulfosporosinus*, *Desulfotomaculum* and *Desulfitobacterium* (Figure 4). The detected genera could reduce the sulfate present in order to form hydrogen sulfide [17,42]. In the equivalent batches with B36 bentonite, no "typical" sulfate reducers were detected. In the respective batches, microorganisms from the genus *Bacillus* were identified, which are known to form spores and to be resistant against harsh conditions [43]. Furthermore, microorganisms from the genera *Marinobacter* were identified in the one-year incubated batches that contained B36 bentonite, CAP solution and substrates (Figure 4). Some species from that genus are known to be resistant against the saline conditions that characterized the respective batches [44].

The results indicate that the microbial "inventory" of the two tested bentonites differed from each other and, thus, also the metabolic potential of the respective microbial species. Further, it is noteworthy that both bentonites contained a high abundance of unknown genera, whose metabolic potential and influence on the mineral assemblages were uncertain. As experiments were conducted under nonsterile conditions, the input of additional microbes could not be excluded. Nonetheless, if active, the detected genera may have influenced the solution chemistry, i.e., by the reduction of sulfate [45]. To assess

if the detected genera led to any changes in smectite structure and composition, purified smectites of supplemented and control samples were analyzed and compared by XRD and SEM–EDX.

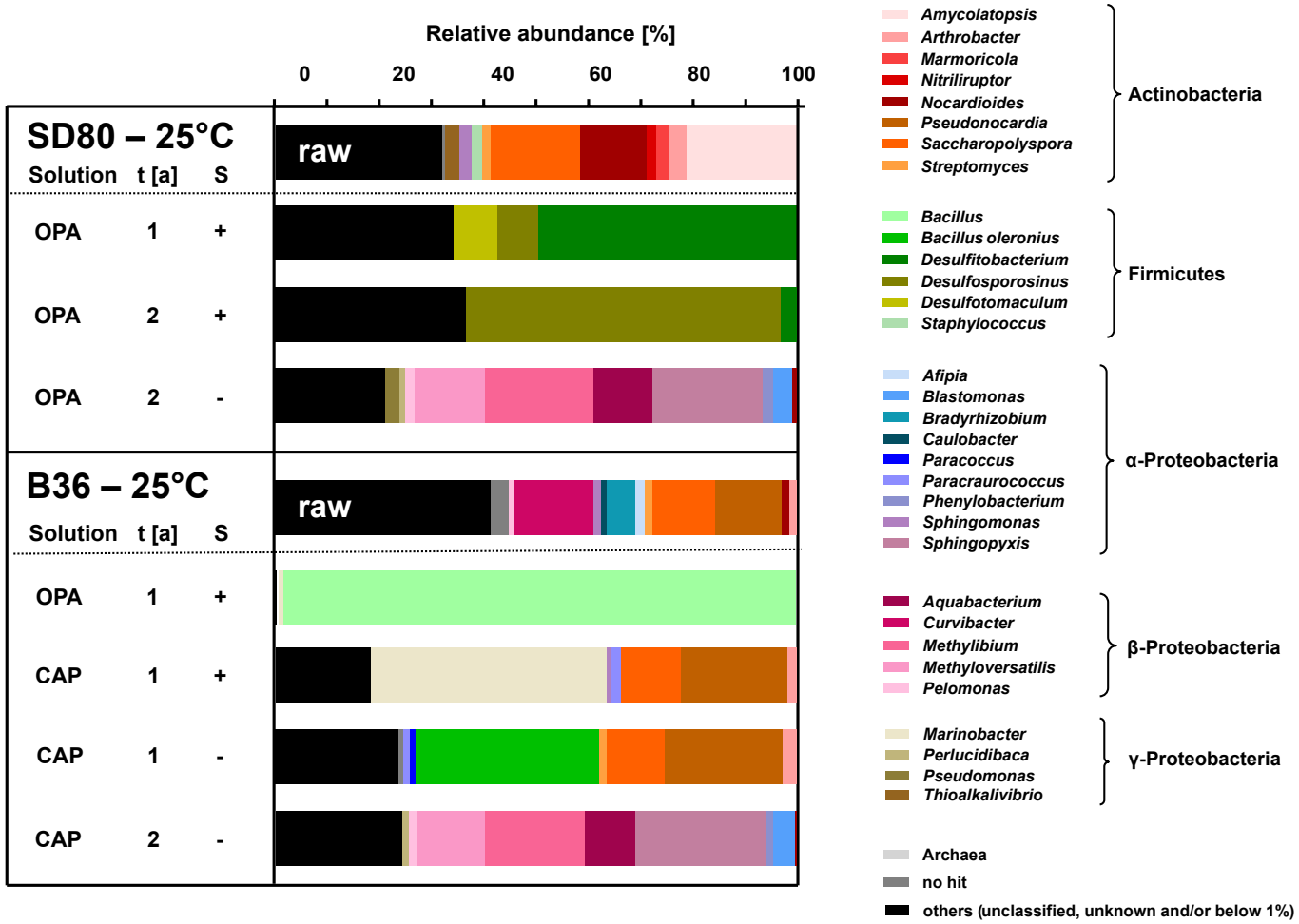

Figure 4. Microbial diversity in B36 and SD80 raw materials and samples incubated at 25 °C. Shown is the relative abundance of detected genera and their dependence on the added substrates (+S) and incubation time (t in years). The microbial community was analyzed by amplifying and sequencing the V4-region of the 16S rRNA gene via MiSeq Illumina (modified from Matschiavelli et al. [26]).

3.2.3. X-ray Diffraction

The random powder XRD patterns of both reacted bentonites showed no neoformed minerals. Minor quantitative differences in the mineralogical composition between the initial and the reacted samples were attributed to heterogeneous sampling. XRD patterns of EG-saturated (001)-reflections revealed some structural differences between samples that were largely independent of the interlayer cation configuration and water content (Tables S7 and S8).

The SD80 samples subjected to OPA solution did not show significant changes in FWHM or d values over time or with increasing temperature (Figure 5a,b). The d_{001} values were at 1.69 nm, and the FWHM ranged between 0.5 and 0.6 Δ° 2θ. However, the XRD patterns of SD80 treated with CAP solution (Figure 5c,d) did show minor differences with d_{001} values between 1.67 and 1.69 nm, whereby the FWHM was constant at 0.6 Δ° 2θ. Only the d_{001} of SD80 reacted for one year at 90 °C without substrate (–S) showed a more significant shift towards smaller d values with d_{001} = 1.65 nm. Overall, the d_{001} reflection intensity of the reacted SD80 smectites notably decreased with increasing temperature conditions.

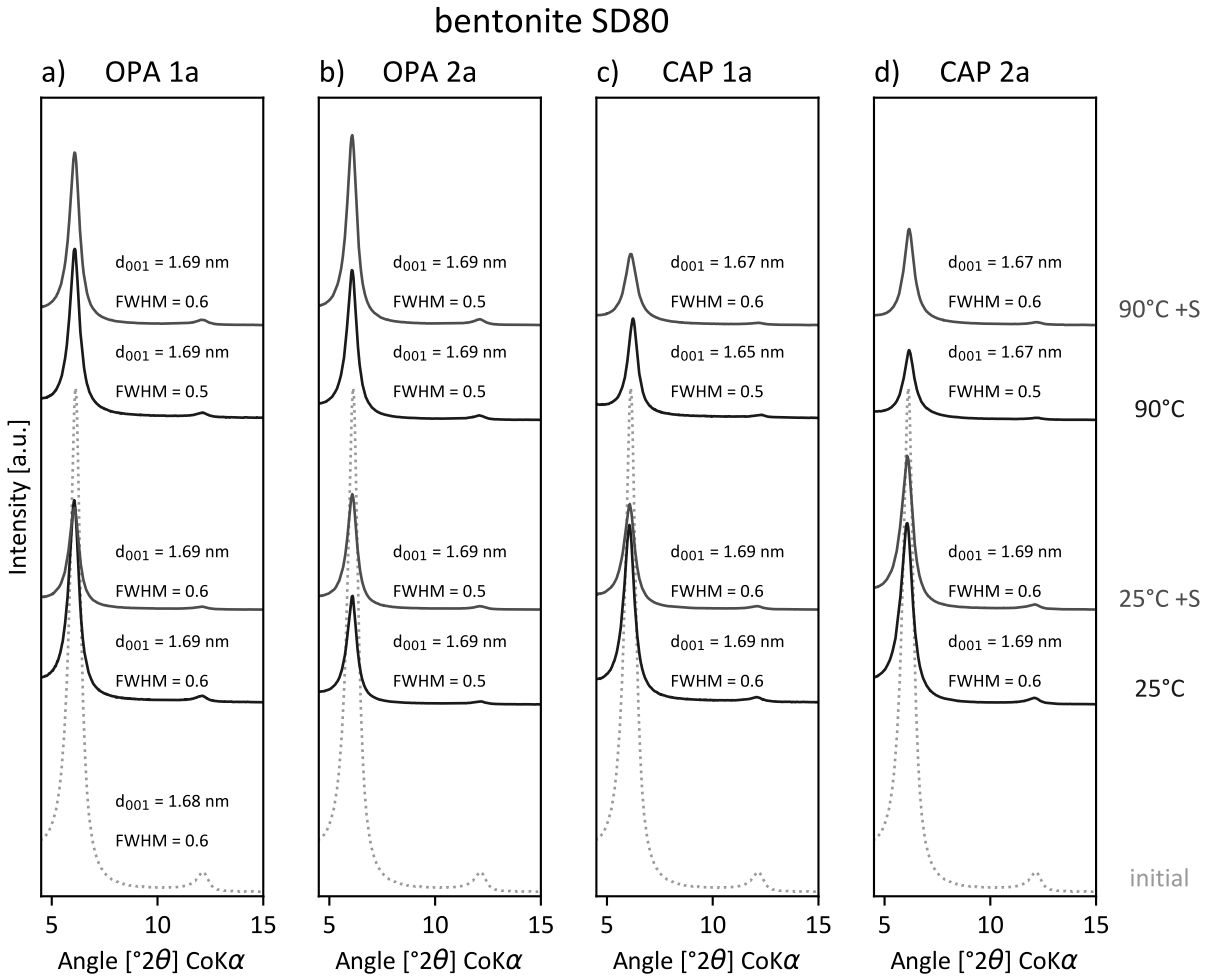

Figure 5. XRD patterns (oriented slides of purified smectite; ethylene glycol-saturated) of the initial SD80 bentonite and reacted samples at two different temperatures (25 and 90 °C) with substrate (+S) and controls. (**a**,**b**) OPA solution for 1 and 2 years and (**c**,**d**) CAP solution for 1 and 2 years. Besides for an overall decrease of reflection intensity, no changes in d-spacing and full-width-at-half-maximum (FWHM) were observed. FWHM in Δ° 2θ. OPA: Opalinus clay pore water, CAP: diluted cap rock solution.

The B36 samples treated with OPA solution did not show significant changes (Figure 6a,b). The (001)-reflection of smectite varied between 1.69 and 1.71 nm, and the FWHM remained constant at 0.8 Δ° 2θ. B36 samples in contact with the CAP solution (Figure 6c,d) showed larger variations in *d* values (1.64–1.72 nm) and FWHM values (0.9–1.1 Δ° 2θ). The highest increase in the FWHM up to 1.1 Δ° 2θ was accompanied by a shift of the d_{001} towards smaller values (1.64 nm and 1.66 nm). This was observed in the two-year sample set reacted at 90 °C both with and without substrate. The increase of FWHM correlating with decreasing *d* values and lower reflection intensities indicates a decrease in crystallite thickness [39], which likely reflects the interlayer exchange of Ca^{2+} by Na^{+} and/or K^{+}.

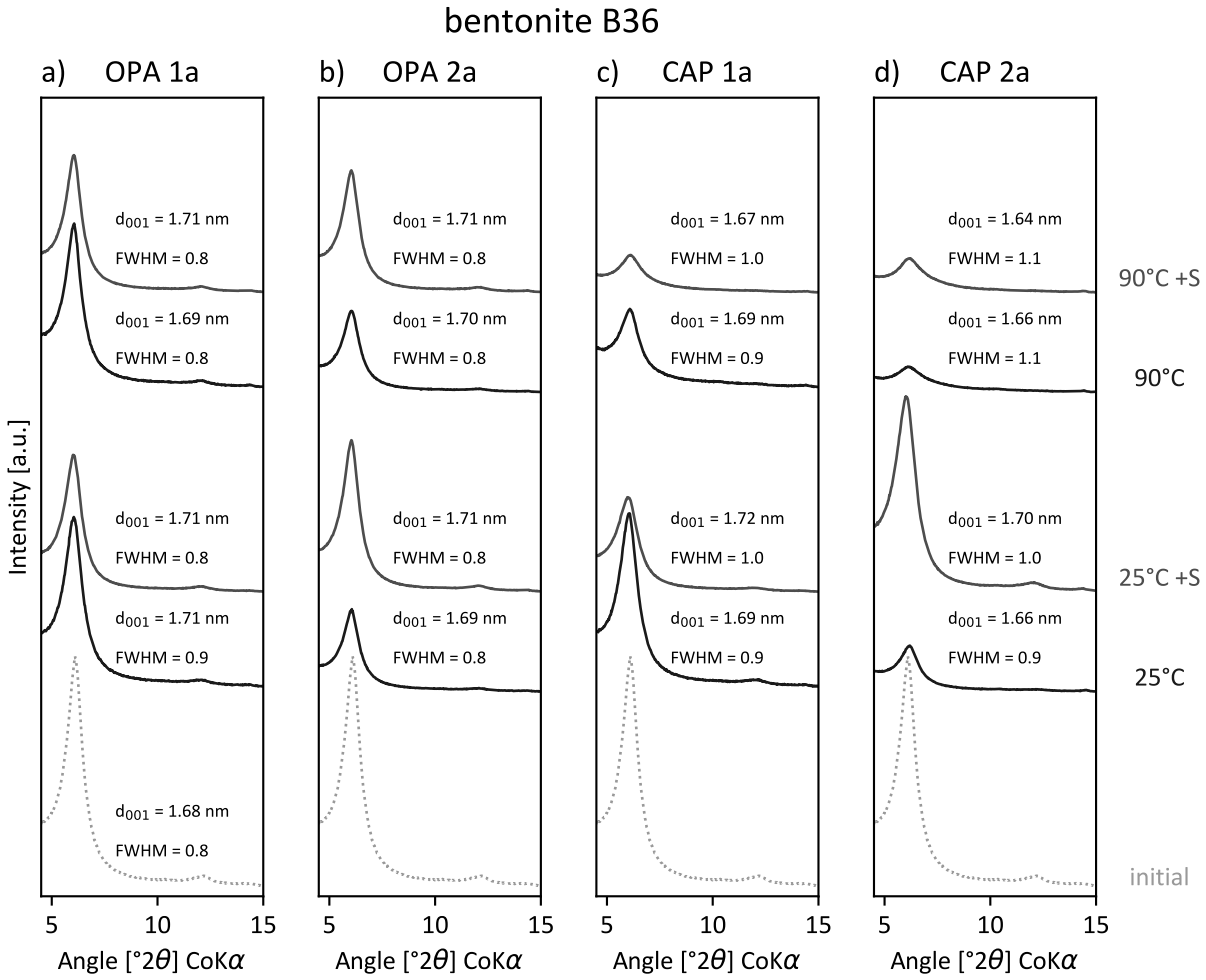

Figure 6. XRD patterns (oriented slides of purified smectite; ethylene glycol-saturated) of the initial B36 bentonite and reacted samples at two different temperatures (25 and 90 °C) with substrate (+S) and controls. (**a**,**b**) OPA solution for 1 and 2 years and (**c**,**d**) CAP solution for 1 and 2 years. Samples reacted in CAP solution show a continuous decrease of $d_{(001)}$ in combination with an increase of FWHM (in Δ° 2θ) with higher temperature and duration. OPA: Opalinus clay pore water, CAP: diluted cap rock solution.

3.2.4. Smectite Layer Charge Distribution

The initial sample of SD80 is classified as a low charged smectite with a total layer charge of −0.36 equivalents per half unit cell (e·phuc^{-1}) and 17% tetrahedral charge (Table 4). The SD80 smectite subjected to OPA solution showed minor changes in the total layer charge with a trend towards elevated layer charges (Figure 7a). The increase in total LC was mainly due to the tetrahedral substitution of Si^{4+} by Al^{3+} along with an overall decrease in octahedral Fe^{3+} and an increase in octahedral Mg^{2+}.

Smectite samples of SD80 treated with CAP solution showed commonly increased layer charges by up to 0.05 e·phuc^{-1} (Figure 7b). Overall, only minor changes in octahedral Mg^{2+} (−0.01 to +0.02 e·phuc^{-1}) and octahedral Fe^{3+} (−0.05 to 0.00 e·phuc^{-1}) were observed for SD80 smectites in CAP solution. Changes in the total layer charge were mainly attributed to the tetrahedral substitution of Si^{4+} by Al^{3+}, which was observed for four samples with a layer charge difference higher than 0.04 e·phuc^{-1}. This includes three substrate-bearing samples (one-year samples at 25 °C; two-year samples at 25 °C and 90 °C) and one sample reacted for two years at 90 °C without substrate that did not show an additional increase in octahedral Al^{3+}.

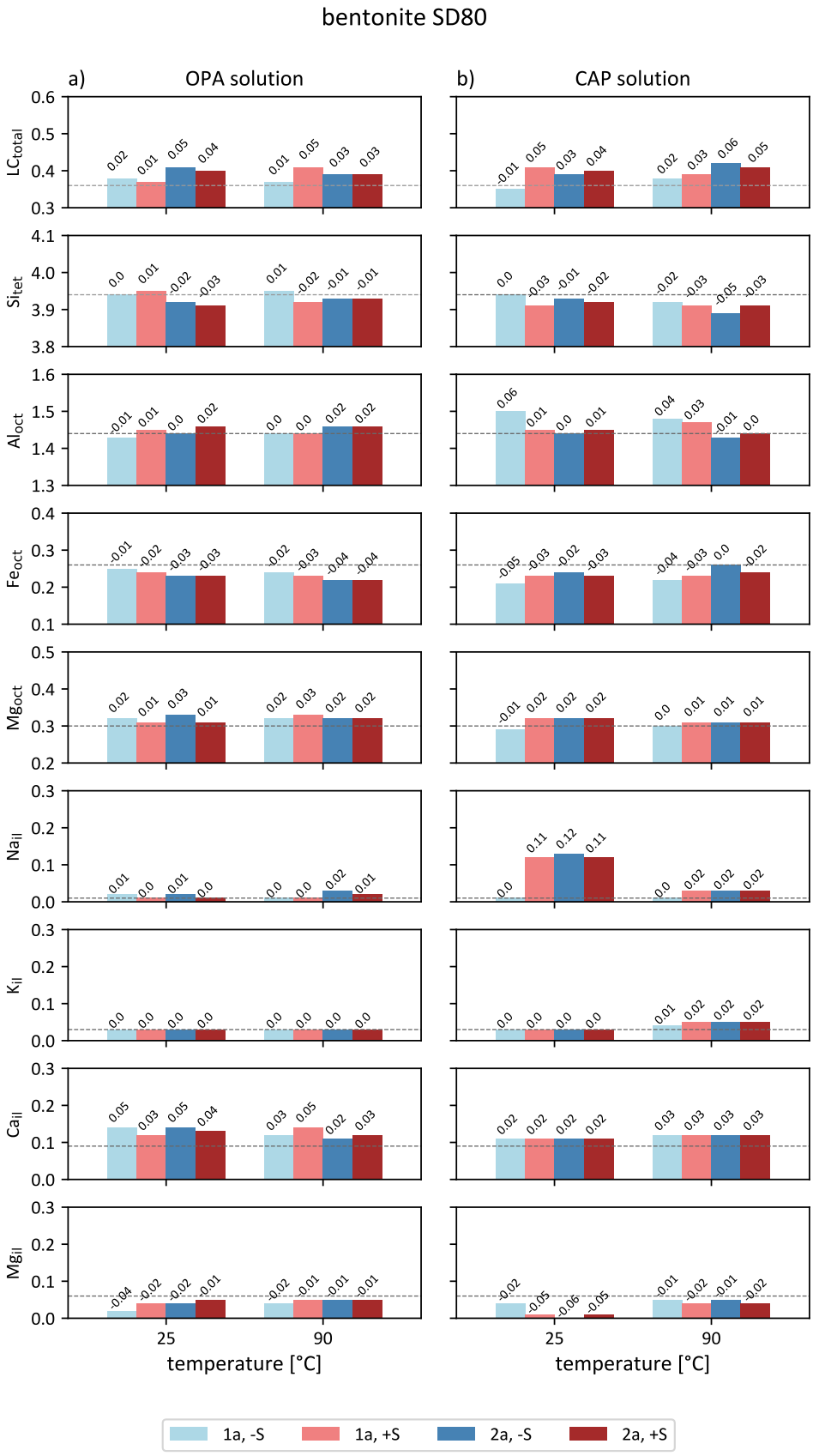

Figure 7. Layer charge and cation distribution of SD80 batch experiments with (**a**) OPA solution and with (**b**) CAP solution; tet: tetrahedral sheet, oct: octahedral sheet, il: interlayer. Values above the bars are displaying the rounded deviation (in e·phuc^{-1}) from the initial sample (dotted line).

The EDX-based structural formula was also used to determine the interlayer cation distribution. The interlayer of the initial SD80 smectite was dominated by Ca^{2+} (0.09 e·phuc^{-1}) and Mg^{2+} (0.06 e·phuc^{-1}), followed by small amounts of K^+ (0.03 e·phuc^{-1}) and Na^+ (0.01 e·phuc^{-1}) (Table S9). In contact with the OPA solution, only minor changes in Na^+, K^+ and Mg^{2+} content were observed, with differences of up to ±0.02 e·phuc^{-1} (Figure 7a). An exception was the one-year control sample reacted at 25 °C, which showed a decrease of 0.04 e·phuc^{-1} for Mg^{2+}. Overall, the Ca^{2+} content increased between 0.02 e·phuc^{-1} and 0.05 e·phuc^{-1}.

In contrast, the SD80 samples subjected to CAP solution showed an uptake of Na^+ into the interlayer with a decreasing amount of substitution with increased temperature (Figure 7b). Compared to the initial sample, the Na^+ in bentonites reacted at 25 °C increased by 0.11–0.12 e·phuc^{-1}. The only exceptions were the one-year control samples reacted at 25 °C and 90 °C, which did not show any differences in Na^+ content. The K^+ content of the 25 °C samples also showed no change, and only minor changes were observed for 90 °C samples with an increase by up to +0.02 e·phuc^{-1}. Overall, enhanced amounts of interlayer Ca^{2+} (0.02–0.03 e·phuc^{-1}) and depleted amounts of Mg^{2+} (0.01–0.06 e·phuc^{-1}) were observed under elevated temperatures.

In comparison, the increased LC in OPA-reacted SD80 samples correlated with the uptake of interlayer Ca^{2+} at 25 °C and 90 °C, whereas in CAP-reacted samples, a constant increase in Ca^{2+} was observed at 25 °C and 90 °C. Additionally, CAP samples at 25 °C showed a noticeable increase in Na^+, which correlated with LC, and a decrease in interlayer Mg^{2+}. At 90 °C, this trend was diminished but accompanied by an increase in K^+. These trends indicate solution-dependent changes whose implications will be discussed later.

The initial sample of B36 is classified as a medium charged smectite with a total layer charge of −0.38 e·phuc^{-1} and 56% tetrahedral charge (Table 4). After treatment with OPA solution, no or only minor changes (0.00 to −0.04 e·phuc^{-1}) in the total layer charge were observed for the two-year samples reacted at 90 °C and the one-year sample sets. Only the two-year samples reacted at 25 °C showed increased layer charges by up to 0.05 e·phuc^{-1} (Figure 8a). The latter are related to tetrahedral substitution of Al^{3+} by Si^{4+} along with an octahedral substitution of Al^{3+} by Fe^{3+}, which results in an overall increase of tetrahedral charge (up to 0.06 e·phuc^{-1}).

The total LC of B36 subjected to CAP solution showed only minor changes at 25 °C, whereas samples reacted at 90 °C had increased layer charges up to 0.06 e·phuc^{-1} in control samples and up to 0.14 e·phuc^{-1} in substrate-bearing samples (Figure 8b). The only exception was the two-year control sample at 25 °C, which showed similar changes compared to the control samples reacted at 90 °C. The 90 °C samples displayed an overall decrease of tetrahedral Si^{4+} between −0.11 e·phuc^{-1} and –0.14 e·phuc^{-1}. Whereas no changes in octahedral charge were observed for the substrate-bearing samples (Fe^{3+} substitutes for Al^{3+}), the octahedral charge decreased up to 0.08 e·phuc^{-1} in the control samples. This was caused by a significant increase of Al^{3+} (up to 0.16 e·phuc^{-1}) along with a decrease of Fe^{3+} (−0.08 e·phuc^{-1}) and Mg^{2+} (up to −0.08 e·phuc^{-1}) in the octahedral sheet.

The interlayer distribution of the initial B36 smectite was dominated by Ca^{2+} (0.11 e·phuc^{-1}) and Mg^{2+} (0.06 e·phuc^{-1}) followed by K^+ (0.03 e·phuc^{-1}) and Na^+ (0.01 e·phuc^{-1}) (Table S10). In OPA solution experiments, the B36 samples showed slight changes in interlayer cation content (−0.03 to 0.02 e·phuc^{-1}) (Figure 8a). The two-year sample set at 90 °C showed enhanced Na^+ contents greater than 0.03 e·phuc^{-1}.

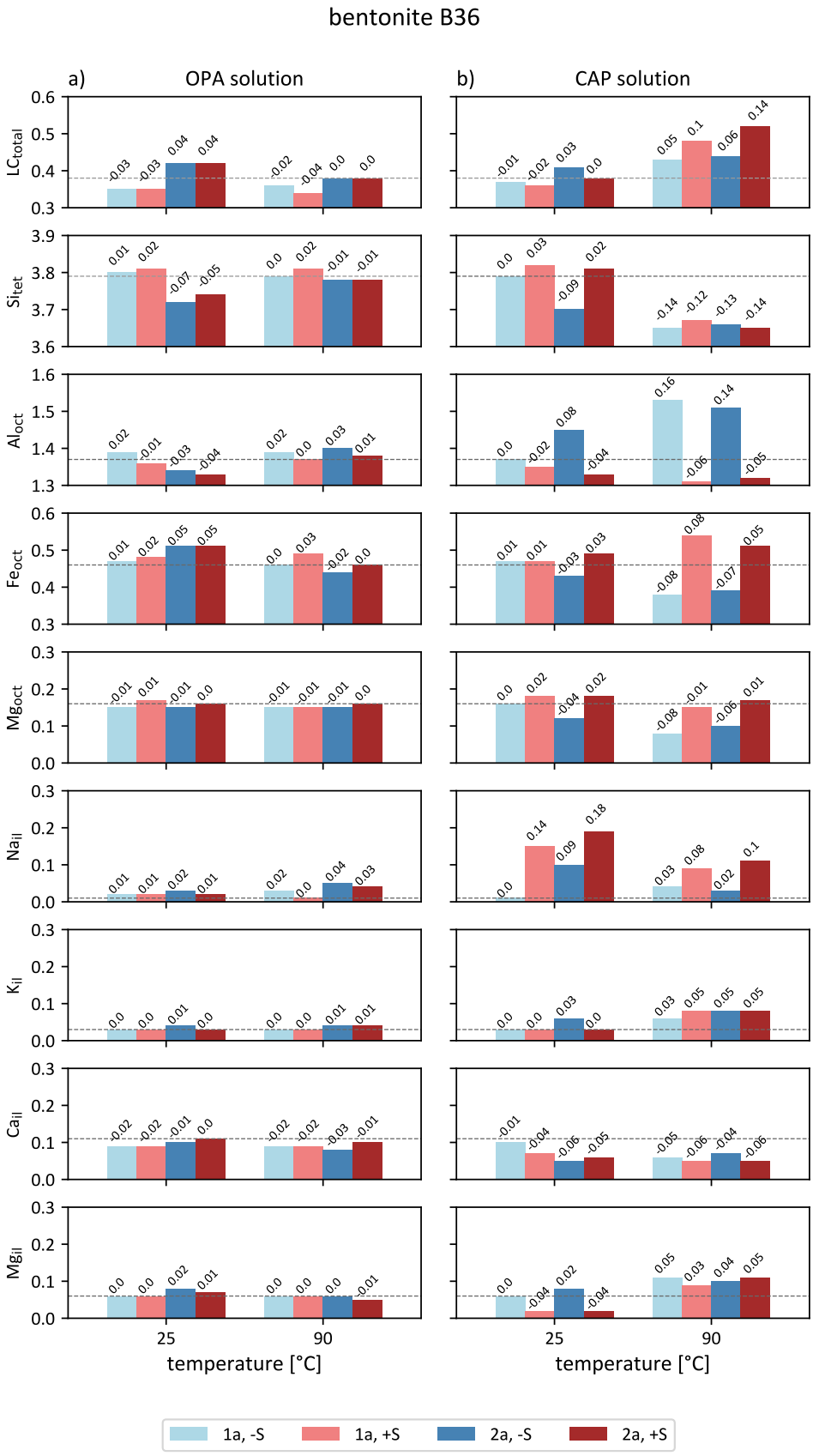

Figure 8. Layer charge and cation distribution of B36 batch experiments with (**a**) OPA solution and with (**b**) CAP solution; tet: tetrahedral sheet, oct: octahedral sheet, il: interlayer. Values above the bars are displaying the rounded deviation (in e·phuc^{-1}) from the initial sample (dotted line).

For B36 samples subjected to CAP solution, an overall uptake of Na^+ cations between 0.08 e·phuc^{-1} to 0.18 e·phuc^{-1} was observed (Figure 8b). The only exceptions were control samples, which reacted for one year at 25 °C, and for the one- and two-year samples reacted at 90 °C, which showed no or only minor increases of up to 0.03 e·phuc^{-1}. A more significant increase of interlayer K^+ between 0.03 e·phuc^{-1} and 0.05 e·phuc^{-1} was observed for the high temperature samples (90 °C) as well as for a control batch reacted for two years at 25 °C. For all samples, the Ca^{2+} content decreased by up to −0.06 e·phuc^{-1}. The amount of interlayer Mg^{2+} increased for the 90 °C samples up to +0.05 e·phuc^{-1}, whereas the substrate-bearing samples at 25 °C showed a decrease in Mg^{2+} of −0.04 e·phuc^{-1}. The control batches reacted at 25 °C showed no or only slight changes (+0.02 e·phuc^{-1}) in interlayer Mg^{2+}.

The most noticeable changes in the B36 bentonite were found in CAP-reacted samples and involved an increased uptake of Na^+ into the interlayer at 25 °C and substrate-influenced tetrahedral and octahedral changes at 90 °C. These changes point towards higher reactivity of B36 in comparison to SD80 and will be discussed in detail later.

As solutions were not renewed during the batch experimentation, a complete exchange of interlayer cations, e.g., Na^+ for Ca^{2+} in contact with the CAP solution was not expected.

3.2.5. Solution Chemistry of the Supernatant

The solution chemistry of the supernatant before and after experimentation was analyzed to estimate the dissolution and cation exchange behavior of both bentonites as well as the change of pH values. During the short-term experiments, pH values for SD80 in OPA solution varied between 7.2 and 7.4 (Table 6). The pH values of SD80 in CAP solution showed an initial decrease from pH = 7.3 to 7.1, which further decreased to pH = 6.9 after 1 day. In contrast, the pH values of B36 were characterized by a strong decrease in both solutions. In contact with OPA solution, the pH immediately decreased from 7.8 to 6.3 within 1 day. Subjected to CAP solution, the pH decreased from 7.3 to 5.7 and remained at 5.0 between 1 and 30 days.

Table 6. Results of pH short-term measurements of both bentonites (SD80, B36) in a glove box at 25 °C with a solid to solution ratio of 1:2. The pH values of both solutions (OPA, CAP) without bentonite are also used as a reference for long-term measurements.

Sample	Solution	0 d	1 d	8 d	30 d
-	OPA	7.8	-	-	-
SD80	OPA	7.4	7.2	7.3	-
B36	OPA	6.3	5.4	5.6	5.7
-	CAP	7.3	-	-	-
SD80	CAP	7.1	6.9	6.9	6.9
B36	CAP	5.7	5.0	5.0	5.0

For long-term experimentation (one and two years), an overall increase of Mg concentrations and an increase of Si concentrations with increasing temperature were observed for all solutions, which indicates temperature enhanced silicate dissolution. Higher Na concentrations in substrate-bearing samples were attributed to the additional input of sodium by Na-lactate and Na-acetate (Tables 7 and 8).

Table 7. Solution chemistry of SD80 bentonite batches and measured pH values (n.d. = not determined due to the complete adsorption of the solution by smectite). DUR: duration, SOL: solution, Su: substrates.

Sample	DUR	T	SOL	Su	pH	Si	Mg	Ca	Na	K	S	Cl
	(a)	(°C)				($mmol \cdot L^{-1}$)	($mmol \cdot L^{-1}$)	($mmol \cdot L^{-1}$)	($mmol \cdot L^{-1}$)	($mmol \cdot L^{-1}$)	($mmol \cdot L^{-1}$)	($mmol \cdot L^{-1}$)
	0	25	OPA	–	7.8	0.1 ± 0.1	14.5 ± 0.6	25.9 ± 1.4	226 ± 11	1.7 ± 0.1	14.7 ± 1.1	308 ± 13
SD80	1	25	OPA	–	n.d.	n.d.	35.0	46.4	274	n.d.	22.1	372
SD80	1	25	OPA	+	n.d.	1.8	41.7	39.7	379	3.1	0.3	n.d.
SD80	1	90	OPA	–	n.d.	n.d.	n.d.	n.d.	n.d.	n.d.	n.d.	n.d.
SD80	1	90	OPA	+	n.d.	n.d.	n.d.	n.d.	n.d.	n.d.	n.d.	n.d.
SD80	2	25	OPA	–	n.d.	0.9	36.3	42.5	254	3.4	21.0	n.d.
SD80	2	25	OPA	+	n.d.	n.d.	n.d.	n.d.	n.d.	n.d.	n.d.	n.d.
SD80	2	90	OPA	–	n.d.	2.5	31.4	56.7	313	6.9	26.2	447
SD80	2	90	OPA	+	n.d.	n.d.	n.d.	n.d.	n.d.	n.d.	n.d.	n.d.
	0	25	CAP	–	7.3	0.2 ± 0.2	n.d.	11.6 ± 3.0	2389 ± 70	6.0 ± 0.6	16.4 ± 0.4	2562 ± 5
SD80	1	25	CAP	–	7.4	0.3	63.2	93.9	2352	7.3	22.1	2642
SD80	1	25	CAP	+	7.4	0.6	82.0	97.7	2773	7.4	23.8	2652
SD80	1	90	CAP	–	7.4	1.3	64.6	113.5	2729	9.5	18.9	2877
SD80	1	90	CAP	+	7.2	1.7	78.0	117.2	2642	10.1	23.6	2750
SD80	2	25	CAP	–	7.4	0.5	69.1	99.3	2481	7.3	23.5	2636
SD80	2	25	CAP	+	7.6	0.7	79.8	96.3	2503	7.7	22.5	2667
SD80	2	90	CAP	–	7.5	1.5	64.9	98.1	2446	10.0	14.6	2907
SD80	2	90	CAP	+	n.d.	1.0	79.9	136.0	2698	9.8	20.5	n.d.

Table 8. Solution chemistry of B36 bentonite batches and measured pH values (n.d. = not determined due to the complete adsorption of the solution by smectite), DUR: duration, SOL: solution, Su: substrates.

Sample	DUR	T	SOL	Su	pH	Si	Mg	Ca	Na	K	S	Cl
	(a)	(°C)				($mmol \cdot L^{-1}$)	($mmol \cdot L^{-1}$)	($mmol \cdot L^{-1}$)	($mmol \cdot L^{-1}$)	($mmol \cdot L^{-1}$)	($mmol \cdot L^{-1}$)	($mmol \cdot L^{-1}$)
	0	25	OPA	–	7.8	0.1 ± 0.1	14.5 ± 0.6	25.9 ± 1.4	226 ± 11	1.7 ± 0.1	14.7 ± 1.1	308 ± 13
B36	1	25	OPA	–	7.3	1.1	28.7	50.9	232	2.5	15.6	353
B36	1	25	OPA	+	6.9	1.4	30.4	60.7	283	2.4	15.9	345
B36	1	90	OPA	–	5.1	2.7	22.5	58.6	231	3.5	14.7	358
B36	1	90	OPA	+	5.2	3.1	25.9	59.3	300	3.1	14.5	347
B36	2	25	OPA	–	7.1	1.1	28.4	58.3	232	2.8	15.1	355
B36	2	25	OPA	+	7.5	1.1	27.7	60.2	282	2.1	11.8	333
B36	2	90	OPA	–	5.0	3.0	27.3	62.0	250	4.5	16.5	385
B36	2	90	OPA	+	5.2	3.2	24.1	55.5	288	3.8	14.6	342
	0	25	CAP	–	7.3	0.2 ± 0.2	n.d.	11.6 ± 3.0	2389 ± 70	6.0 ± 0.6	16.4 ± 0.4	2562 ± 5
B36	1	25	CAP	–	6.7	0.5	35.8	96.1	2351	7.5	16.4	2590
B36	1	25	CAP	+	7.5	0.7	40.9	107.8	2617	7.1	17.6	2621
B36	1	90	CAP	–	4.5	2.2	38.6	107.3	2672	8.4	18.1	2787
B36	1	90	CAP	+	4.7	2.0	36.7	107.6	2637	7.5	17.6	2659
B36	2	25	CAP	–	7.0	0.6	34.5	92.7	2514	6.8	17.5	2576
B36	2	25	CAP	+	7.1	0.7	38.1	93.1	2336	6.9	15.6	2597
B36	2	90	CAP	–	4.6	2.4	37.8	101.1	2575	8.8	15.2	2777
B36	2	90	CAP	+	4.8	2.5	36.2	97.7	2429	7.6	16.3	2615

The pH and most ICP-OES measurements for SD80 in contact with OPA solutions were not feasible due to the complete adsorption of water molecules by smectite particles. SD80 samples reacted in CAP solution showed pH values that varied between 7.2 and 7.6. Solutions of supplemented SD80 samples showed slightly higher Mg concentrations than the control samples. A significant decrease in the S concentration from about 15 mmol·L^{-1} to almost 0 mmol·L^{-1} was observed for the one-year sample reacted at 25 °C in OPA solution (+S) in which sulfate-reducing bacteria were detected as aforementioned (Table 7). Solutions of sample B36 showed decreasing pH values with increasing temperature (Table 8).

4. Discussion

4.1. Smectite Alteration Mechanisms

The structural alteration of the smectite, which was observed in both sets of bentonite experiments, can be attributed to three main mechanisms: (i) interlayer cation exchange, (ii) tetrahedral substitution of Si^{4+} by Al^{3+} and (iii) octahedral substitution of Fe^{3+} and Mg^{2+} by Al^{3+} and to a lesser extent of Al^{3+} by Fe^{3+}. To varying degrees, these mechanisms are controlled by experimental conditions, which are temperature, duration of the experiments, solution chemistry, the mineralogical composition of the bentonites and whether or not the experiments are supplemented with organic supplements. Due to the complexity of the bentonite assemblages and their microbial compositions, it was not possible to differentiate any single parameter as being responsible for the smectite alteration, so probable causes for the observed types of alteration are discussed below.

4.1.1. Interlayer Cation Exchange

The reactivity of bentonites in saline solutions has been studied extensively in the past [10,12,46]. As reported by Kaufhold and Dohrmann [11], the degree of interlayer cation exchange is determined by the ionic strength of the solution and the solid to solution ratio. Although both solutions used in this study are Na-dominated (Table S1), significant Na^+ uptake into the interlayer was only observed for CAP-reacted samples at 25 °C and partly at 90 °C, whereas samples reacted in OPA solution showed only minor interlayer exchange. In comparison to other studies (e.g., [47]), these slight changes are likely to reflect the low solid to solution ratio (1:2) in combination with non-stirred bentonite slurries.

At 90 °C, both smectites reacted in CAP solution showed an increase of interlayer K^+, which indicates an increase of collapsed layers. For B36, this is supported by the trends observed for EG-saturated 001-reflections (Figure 9), which show a continuous decrease of $d_{(001)}$ in combination with an increase of the FWHM at higher temperature and longer duration. This points towards a decrease in X-ray scattering domain sizes, which likely resulted from particle delamination [39]. Delamination is known to occur during the interlayer exchange of Ca^{2+} by Na^+ when treated with NaCl-dominated saline solutions [48]. This is supported by the continuous decrease of basal spacing in combination with an increase of FHWM with both temperature and duration for sample B36. This effect is intensified in the presence of the organic substrate, which also contained higher amounts of Na^+ in the interlayer compared to the control samples (Table S10), which was possibly derived from the added Na-lactate and Na-acetate.

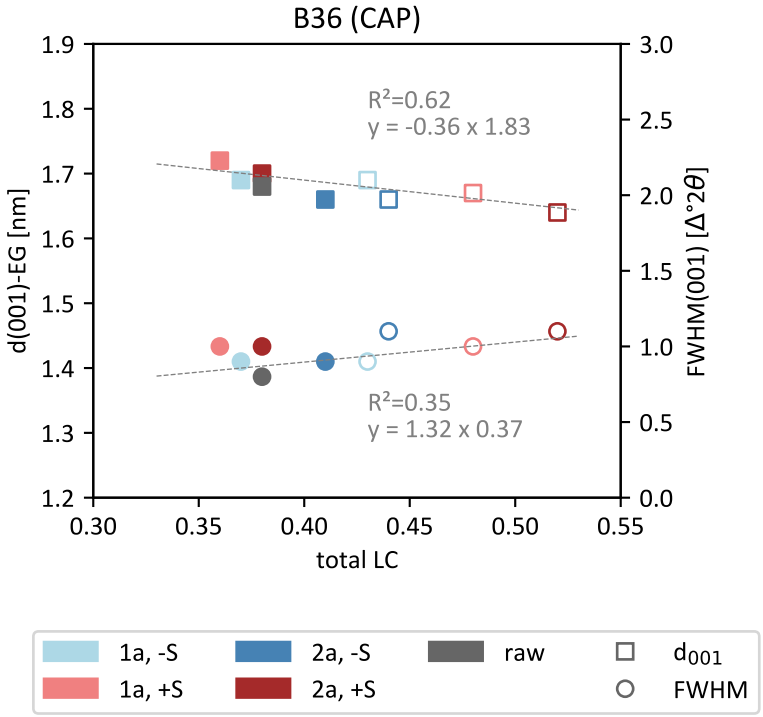

Figure 9. Plot of 001-reflection parameters against layer charge of ethylene glycol-saturated B36 samples reacted in CAP solution at 25 °C (circle filled) and 90 °C (circle unfilled). FWHM: full-width-at-half-maximum, LC: layer charge, –S: without substrate, +S: with substrate.

As layer charge is known to influence smectite colloidal properties, an increase in the total layer charge can lead to a decrease in crystalline swelling [49,50], whereby the swelling also decreases with increasing salinity of the respective pore water [46]. However, the changes in the 001-reflection (intensity, position, FWHM) of EG-saturated smectites are largely attributable to the reversible effects of interlayer cation exchange and particle delamination and therefore are not considered to represent a permanent structural change.

In comparison to B36 samples reacted at 25 °C, the 90 °C samples showed a significant decrease of the pH to values between 5.0–5.2 (OPA) and 4.5–4.8 (CAP), which was independent of the addition of substrate (Table 8). Kaufhold et al. [51] argued that the hydrolysis of exchanged interlayer Ca^{2+} could lead to a minor decrease in pH values. However, an increase of Ca^{2+} in both solutions was observed for all samples. Although no carbonate phases were detected by XRD in the bulk materials, minor amounts were found in other studies (SD80: 2.8 wt.%, B36: 0.35 wt.%) [25] and, if present in small amounts in these samples, could further explain the increase in Ca^{2+}. Therefore, interlayer Ca^{2+} or any additional Ca^{2+} in the solution is not considered to be the likely source of acidification. Beaufort et al. [52] observed decreasing pH values in hydrothermal experiments at 200 °C with purified smectites, which indicates that the alteration of smectite itself could influence the solution pH. However, the exact source of acidification remains unclear but is possibly related to deprotonation reactions that may occur during heating [53] and/or to the potential reduction of octahedral Fe^{3+}. The latter can lead to the adsorption of dissociated H_2O, whose H^+ can be subsequently substituted by Na^+ [54]. The decrease in pH likely did not result in enhanced montmorillonite dissolution, as dissolution rates within the observed pH range are generally of the same order of magnitude [55].

4.1.2. Tetrahedral and Octahedral Charge Distribution

The determination of the layer charge distribution based on EDX analyses can provide information about the early stage alteration of smectites, which cannot be detected or differentiated in the analyses of the bulk material (XRD, XRF). The interpretation of structural changes solely based on the total layer charge must be taken with caution, as elemental

changes <0.02 e·phuc^{-1} lie within the margin of error, and these errors will accumulate when summing up the total charge. As a result, more reliable interpretations are made by considering the charge distribution (Figures 10 and 11). During smectite alteration in the bentonite-solution experiments, a layer charge increase mainly occurred as a result of tetrahedral substitution of Si^{4+} by Al^{3+}, as observed in both samples. A correlation between the increasing degree of smectite alteration and reaction time was observed in both SD80 and B36 bentonites reacted in OPA solutions at 25 °C. While both samples showed no alteration of the tetrahedral sheet after one year, a slight but significant decrease in tetrahedral Si^{4+} was detected after two years both with and without substrate. The tetrahedral (TET) and octahedral (OCT) charge of samples reacted in OPA solution at 90 °C differed only slightly from the initial sample.

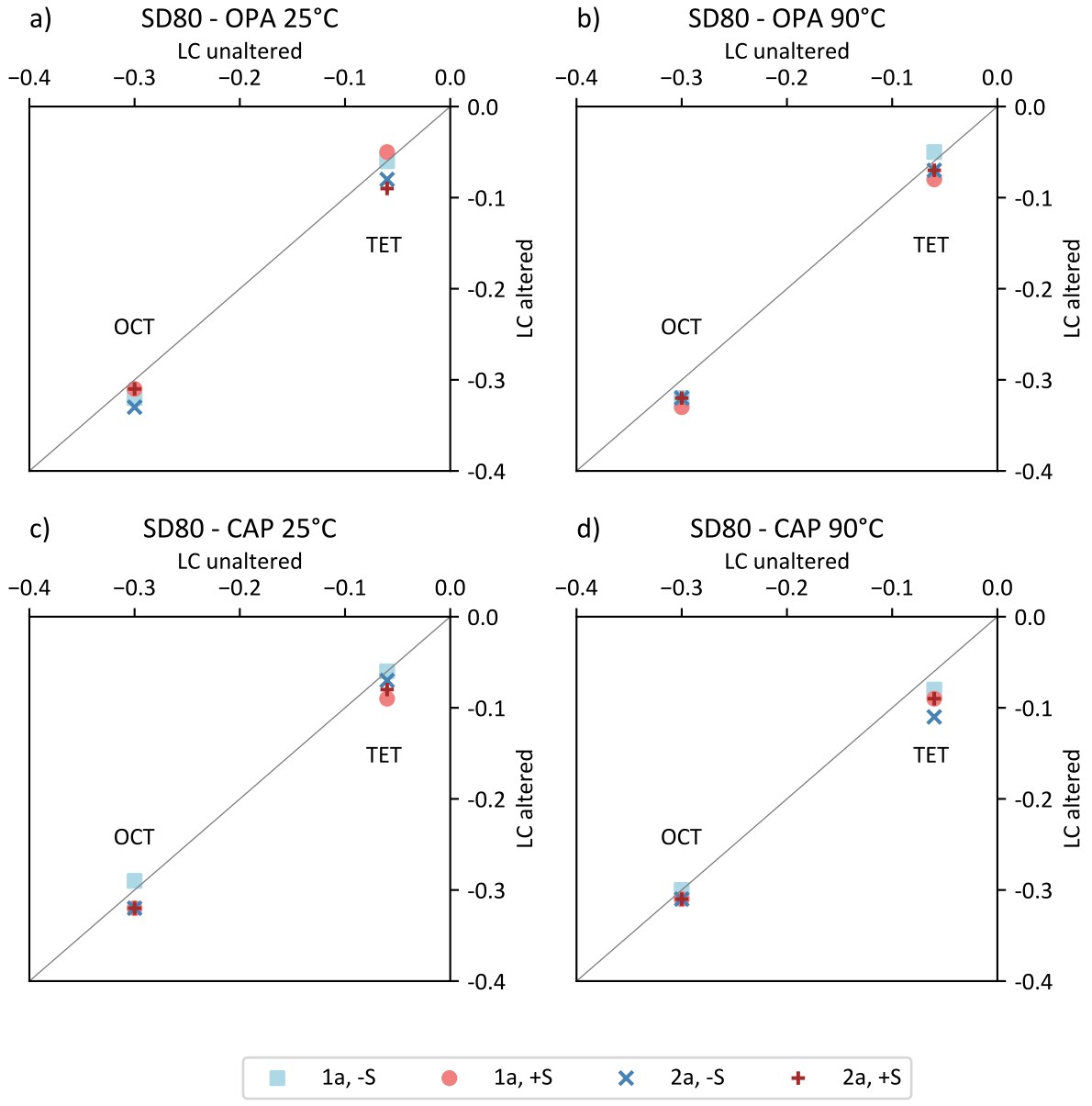

Figure 10. Scatter plots for SD80 smectites that compare the altered tetrahedral (TET) and octahedral (OCT) charges to the initial charge distribution for samples reacted in (**a**,**b**) Opalinus clay pore water (OPA) and (**c**,**d**) diluted cap rock solution (CAP). Overall, only minor changes were observed after experimentation. LC: layer charge, −S: control samples without substrate, +S: samples with substrate.

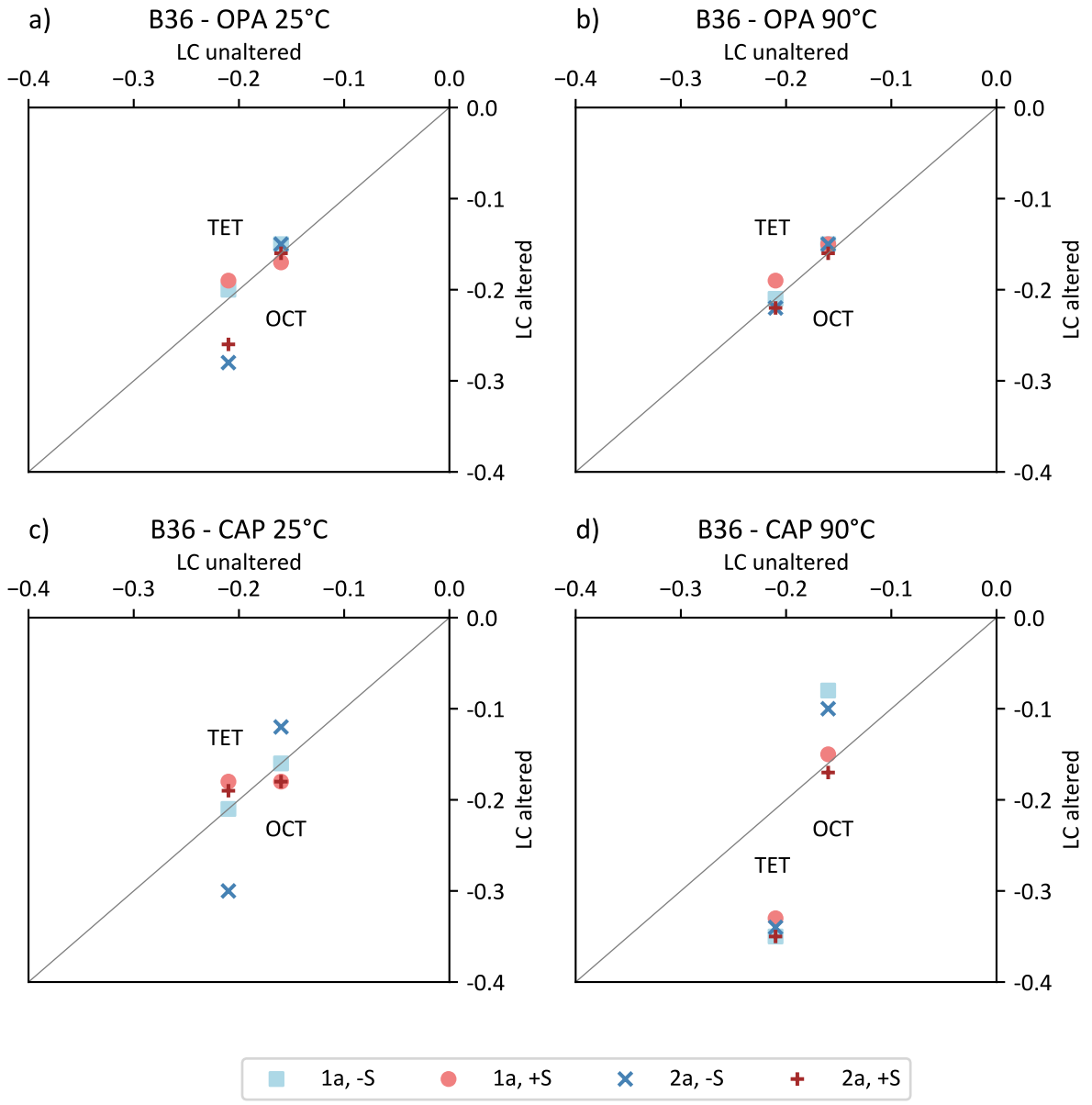

Figure 11. Scatter plots for B36 smectites that compare the altered tetrahedral (TET) and octahedral (OCT) charges to the initial charge distribution for samples reacted in (**a**,**b**) Opalinus clay pore water (OPA) and (**c**,**d**) diluted cap rock solution (CAP). An increase of the tetrahedral charge was observed for samples reacted in OPA solution at 25 °C after two years (**a**) and in the corresponding control sample reacted in CAP solution (**c**). B36 samples reacted in CAP solution at 90 °C show the highest changes, with an overall increase in tetrahedral charge along with a decrease in octahedral charge for the control samples. LC: layer charge, –S: control samples without substrate, +S: samples with substrate.

Where sample SD80 generally showed only minor variations (Figure 10), more significant changes were seen in the B36 bentonite, especially when subjected to CAP solution at 90 °C (Figure 11d). It should be noted that the control sample reacted at 25 °C after two years showed similar changes as the equivalent sample at 90 °C (Figure 11c). In contrast to MX80 studies by Herbert and co-workers [10], no surplus of Si was observed, indicating montmorillonite alteration toward kaolinite or pyrophyllite compositions as favored in closed systems. In this sample set, a significant increase in the tetrahedral layer charge due to substitution of Si^{4+} by Al^{3+} was detected. This resulted in an overall increase of layer charge and an alteration toward a beidellite reaction product. The additional Al needed for this "beidellitization" process may be provided by the localized dissolution and

precipitation of montmorillonite [56] or by the dissolution of accessory minerals, such as unstable feldspar grains [57].

Considering the octahedral charge distribution, differences between control and supplemented samples were observed. Thus, the control samples displayed a significant increase in tetrahedral charge, along with a decrease of octahedral charge, due to the Fe^{3+} and Mg^{2+} substitution by Al^{3+}. This indicates the formation of high charged beidellitic layers ($\xi \geq 0.43$ e·phuc^{-1}, TET: 77–81%). Whereas, the substrate-bearing samples, with the overall highest layer charges ≥ 0.48 e·phuc^{-1}, showed a similar increase of tetrahedral charge (TET: 67–69%), there was little change in the octahedral charge. Here, the octahedral Al^{3+} was substituted by Fe^{3+}, and the interlayer Na^{+} was slightly increased.

Beaufort and co-workers [52] found that the formation of beidellitic smectite is accompanied with the release of excess Mg in solution, which subsequently led to the formation of trioctahedral smectite. However, no evidence for trioctahedral precipitates was found in the XRD patterns of this study (e.g., d_{060} reflection remained at 0.150 nm).

Although higher resolution SEM images (30,000-fold magnification) and XRD studies of the purified samples showed no indication of nanoparticle contamination, traces of accessory silicate phases (e.g., amorphous silica, cristobalite) cannot be fully ruled out. If present, they would result in Si-contamination of the compositional analyses. As the amount of Si detected in the purified smectite fraction was in most cases not sufficient to fill all tetrahedral metal sites (4 atoms per unit formula), it is assumed that the effect of any impurities was negligible and had no or little influence on the smectite compositions presented. Furthermore, random powder XRD measurements showed no formation of new minerals occurred during experimentation, which may interfere with analyses of the purified fractions.

Due to the different natures of the two bentonites studied, including their different smectite compositions, it is considered likely that the smectites, which were both subjected to the same experimental conditions, reacted differently in each material. In this context, the low charged SD80 as a beidellitic montmorillonite showed nearly no structural change, whereas B36, as a medium charged montmorillonitic beidellite, became more beidellitic with increasing temperature and reacted in the highly saline CAP solution. This corresponds to the findings of Nguyen-Thanh and co-workers [58], who suggested that reactivity of smectite increases with a higher degree of octahedral substitution. Furthermore, reactions with accessory minerals (e.g., K-feldspar, pyrite, calcite), the abundance of which varied between the bentonites, are also likely to have affected the smectite alterations, although such effects could not be determined in this study.

4.2. Microbial Diversity and Its Potential Influence on the Mineralogy

Microbial activity in a future HLW repository may influence the bentonite barrier performance by various processes, such as leading to potential gas and sulfide production or changes in redox potential [45]. Considering the results of EDX analyses, no microbial induced smectite alteration was observed in batches treated with substrate. Although the experimental setup was prepared under nonsterile conditions and with a diversity of substrates, the results of extracted DNA indicate that the batches did not develop diverse assemblages of microorganisms. Thus, the applied conditions favored the formation of specialized microorganisms that could adapt to these conditions. The detected genera, which dominated especially the SD80 slurry experiments with OPA solution, have been found in former bentonite slurry experiments [59,60], indicating that these microorganisms originated from the SD80 bentonite.

In general, bentonites are known for their low biomass [23], so that the concentration of extracted DNA was very low (Table S6). The DNA extraction was also hindered by the adsorption of negatively charged DNA to the cationic surfaces of the smectite particles, a mechanism enhanced with decreasing pH due to the increase in positively charged edge sites [61,62].

However, SD80 samples treated with substrate and reacted at 25 °C in OPA solution showed the highest amount of extracted DNA. Within these samples, spore-forming and sulfate-reducing bacteria are dominant. The latter are able to reduce sulfate in order to form H_2S [17,42], which is known for promoting metal corrosion [17,18]. The formation of black spots in the respective sample could be an indication of FeS precipitation (Figure 3a), as similarly observed by Pedersen and co-workers who found a blackening of suspensions with a pH between 7 to 5 [19]. However, these black spots are local precipitates that were not detectable in the sampled material by XRD or SEM–EDX techniques.

The extreme conditions found in saline pore waters (e.g., CAP solution) promote the dominance of specialized microorganisms, i.e., the dominance of *Marinobacter* and *Bacillus* species in the respective B36 samples. Although no smectite alteration in correlation with microbes occurred, color changes in the substrate-bearing B36 batches could be an indication of Fe^{3+} reduction (Figure 3d) [41]. In short-term experiments (98 days, 30 °C) with B36 reacted in OPA solution, the green coloration of the bentonite and supernatant pore water was also observed by Matschiavelli et al. [26]. Moreover, the measurements of the iron concentrations showed an increase of Fe^{2+} and a decrease of Fe^{3+} [26].

Although no typical iron-reducing bacteria were detected within the sample sets studied, other non-identified species as well as some of the detected genera (e.g., *Bacillus* [63]) may change the Fe oxidation state due to changing redox conditions or by direct or indirect iron reduction via AQDS [64,65]. This may lead to layer charge increases [56] and the consequences described in Section 4.1.1. Such changes, however, will not be detected by the EDX method applied in this study, which assumes all iron to be in the Fe^{3+} state.

In general, the utilized organic substrates lactate, acetate and methanol are used for various anaerobic metabolisms as the energy sources [66–68], whereas the humic analogue AQDS serves as an electron shuttle [64]. It should be noted that the concentrations of the substrates added to the batches are higher compared to those expected in a natural bentonite environment or in the deep geological repository itself. To accelerate the microbial processes and to shorten the incubation period, the concentration was increased without knowing whether the tolerable concentration would be exceeded. Matschiavelli et al. [37] pointed out that a lactate or acetate concentration of 50 mM is possibly too high for soil organisms, which is also likely for the organic mixture concentrations used in this study. Inherent microorganisms may be affected, since they are not used to coping with these high concentrations in their natural environment. However, a general mix of substrates at lower concentrations is more relevant to a future deep geological repository setting, since it has been shown that organics such as lactate, acetate, formate and malate are present in pore waters that can potentially enter the repository [69]. Considering the respective environmental conditions, the addition of the correct concentrations of natural organic and humic acids to bentonite needs to be optimized in future experiments as potential substrates and electron shuttles for stimulating microbial metabolisms.

4.3. Implications for a Real Repository Scenario

The static batch-experiments with bentonite slurries performed in this study are not representative for the initial conditions of a repository site in terms of the degree of compaction, where tight pore space and low hydraulic conductivities will limit transport processes [13]. However, the importance of these experiments to the long-term performance of the bentonite barrier is considered to be relevant. Over time, niches in the repository are likely to form, where erosion and particle transport will lead to less compacted material [14]. This may result from the infiltration of groundwater through fissures or cavities and along contact zones, leading to the development of localized bentonite clay slurries and changing environmental conditions (e.g., salinity, pH), which may affect the bentonites stability.

Within the experimental period, no clear evidence for mineral transformations (e.g., smectite-to-illite conversion) of the smectite samples was observed. However, for the B36 smectite reacted at 90 °C in higher saline CAP solutions, an uptake of interlayer K^+ is recognizable. This is accompanied by an increase in layer charge, which is an initial step

that could lead to the fixation of potassium. Additionally, XRD results point towards a decrease in swelling capability, which is indicated by lower *d* values and broader basal reflections (FWHM) in the respective samples (Figure 9). These findings indicate that in long-term experiments, illitization may possibly take place, which would lead to a reduction or even a loss in the swelling and sealing capacity of the bentonite buffer.

Kaufhold and Dohrmann [4] highlighted several key factors that make a bentonite less suitable for HLW disposal. These included mineral alteration, loss of swelling capability, availability of soluble or reactive phases (such as pyrite or gypsum), a high structural Fe content in the smectite as well as a high layer charge density. Considering these parameters, our mineralogical results indicate that the Fe-rich montmorillonitic–beidellite B36 bentonite with its higher abundance of accessory minerals (~35 wt.%) is likely to be less suitable as barrier material than the bentonite SD80 with beidellitic–montmorillonite as the main component (~90 wt.%). In this context, the B36 material showed clear signs of becoming more beidellitic when reacted at higher temperatures in the diluted cap rock solution compared to the SD80 bentonite that showed close to no structural change in any of the experiments conducted. As the highest increase in layer charge was observed for the substrate-bearing B36 samples at 90 °C in CAP solution, the addition of organic and humic acids that can act as electron-donors and promote protonation/deprotonation surface reactions [70] may well have contributed to this advanced state of alteration.

The relevance of microbial activity to the repository scenario, based on similar 1-year bentonite slurry experiments, has been previously discussed [37]. Indigenous microorganisms were shown to evolve under different temperature and substrate conditions but had no significant effect on the analyzed biogeochemical parameters [37,71]. In this follow-up study on two different bentonites, similar slurry experiments with an additional focus on mineralogical changes were compared with and without the addition of organic supplements. Similar microbial results were obtained when adding substrate, but the detected genera did not appear to significantly affect the mineralogical properties of the SD80 and B36 bentonites within the two years of experimentation at low temperatures. A notable result was also the very low amount of DNA in samples reacted in CAP solution or in OPA solution without organic supplements. This emphasizes the point that the availability of nutrients and the salinity are likely to be limiting factors for growth in a slurry environment. It is therefore important in future experimental studies to investigate more nutrient poor systems in waters of variable salinity over time periods of several years in order to gain a more accurate understanding of the potential influence of microbes in the long-term repository setting.

5. Conclusions

Static batch experiments were carried out for one and two years at 25 °C and 90 °C using two different bentonites (SD80 from Greece, B36 from Slovakia) and two types of saline solutions, which simulated (a) Opalinus clay pore water with a salinity of 19 $g \cdot L^{-1}$ and (b) diluted cap rock solution with a salinity of 155 $g \cdot L^{-1}$. The bentonites were supplemented with and without organic substrates to study the microbial diversity and their potential influence on the bentonite mineralogy.

1. After experimentation, no neoformation of minerals was observed. Mineralogical and chemical changes can be attributed to interlayer cation exchange reactions, particle delamination and tetrahedral as well as octahedral metal ion substitutions. These changes are more pronounced at higher salinity and elevated temperatures.
2. The initial charge distribution determines the reactivity of the smectite, with octahedral charge dominated smectites (e.g., SD80) being less susceptible to these alterations. However, the influence of accessory minerals (e.g., feldspar, calcite, pyrite) on the environment and smectite alteration should not be neglected with regard to the long-term stability of the bentonite barrier.
3. Considering the microbial influence on a potential HLW repository, the detected genera in SD80 appear to be more important than the specialized microorganisms

detected in bentonite B36 due to their potential to reduce sulfate in order to form H_2S, and thus, promoting the corrosion of metal canisters. Further, it should be noted that the microbial diversity changed with respect to the bentonite and to the applied conditions used in this study. As a result, bentonite-inherent microorganisms may have a potential negative long-term effect on the barrier system. This should be considered when selecting bentonites as buffer material.

4. The reaction kinetics of smectite alteration as well as the precise role of microbes could not be determined due to the complexity of bentonite mineral assemblages and the large number of influencing factors. Further experimentation using simpler mineral mixtures and the addition of single substrates (hydrogen gas, lactate or acetate) at lower concentrations are required. The measurement and quantification of metabolites, e.g., the formation and consumption of organic acids and gases, is necessary to understand further the microbial metabolic potential within the bentonites and its impact on the barrier system.

Supplementary Materials: The following are available online at https://www.mdpi.com/article/10.3390/min11090932/s1, Table S1: Recipes for synthetic OPA and CAP solution, Table S2: XRF results of SD80, Table S3: XRF results of B36, Table S4: EDX raw data SD80, Table S5: EDX raw data B36, Table S6: Concentrations of extracted DNA (ng/µL), Table S7: XRD results of SD80, Table S8: XRD results of B36, Table S9: EDX-based SF SD80, Table S10: EDX-based SF B36

Author Contributions: Conceptualization, C.P., L.N.W., G.G., A.C., T.A., A.M.; methodology, C.P., L.N.W., N.M., A.C.; validation, C.P., N.M., M.P.; formal analysis, C.P.; investigation, C.P., N.M., S.K.; resources, A.M., L.N.W., G.G., T.A., A.C., N.M.; writing—original draft preparation, C.P., L.N.W., N.M.; writing—review and editing, all authors; visualization, C.P., N.M., M.P.; supervision, L.N.W., G.G., A.C.; project administration, L.N.W., T.A., A.M.; funding acquisition, L.N.W., T.A., A.M. All authors have read and agreed to the published version of the manuscript.

Funding: This research is part of the joint project "UMB" funded by the Federal Ministry of Economic Affairs and Energy (BMWi) under the grant number 02 E 11344C. We also acknowledge the support for the Article Processing Charge from the DFG (German Research Foundation, 393148499) and the Open Access Publication Fund of the University of Greifswald.

Institutional Review Board Statement: Not applicable.

Informed Consent Statement: Not applicable.

Data Availability Statement: The data presented in this study are partially available upon request from the corresponding author.

Acknowledgments: We would like to thank Manfred Zander (UG) for the introduction to electron microscopy and its sample preparation, Veronika Prause (GRS) for the batch preparation and pH measurements, Karin Grupe (GRS) for ICP-OES measurements, Jennifer Drozdowski (HZDR) for her help with sampling and Stephan Kaufhold (BGR) for providing the bentonites.

Conflicts of Interest: The authors declare no conflict of interest.

References

1. Gilg, H.A.; Kaufhold, S.; Ufer, K. Smectite and bentonite terminology, classification, and genesis. In *Bentonites: Characterization, Geology, Mineralogy, Analysis, Mining, Processing and Uses*; Kaufhold, S., Ed.; Schweizbart Science Publishers: Stuttgart, Germany, 2021; ISBN 978-3-510-96859-6. in press.
2. Christidis, G.E.; Huff, W.D. Geological aspects and genesis of bentonites. *Elements* **2009**, *5*, 93–98. [CrossRef]
3. Sellin, P.; Leupin, O.X. The use of clay as an engineered barrier in radioactive-waste management—A review. *Clays Clay Miner.* **2013**, *61*, 477–498. [CrossRef]
4. Kaufhold, S.; Dohrmann, R. Distinguishing between more and less suitable bentonites for storage of high-level radioactive waste. *Clay Miner.* **2016**, *51*, 289–302. [CrossRef]
5. Savage, D. An Assessment of the Impact of the Degradation of Engineered Structures on the Safety-Relevant Functions of the Bentonite Buffer in a HLW Repository. NTB-13-02, Wettingen, Switzerland. 2014. Available online: https://inis.iaea.org/search/search.aspx?orig_q=RN:48088313 (accessed on 21 June 2021).

6. Kaufhold, S.; Klimke, S.; Schloemer, S.; Alpermann, T.; Renz, F.; Dohrmann, R. About the corrosion mechanism of metal iron in contact with bentonite. *ACS Earth Space Chem.* **2020**, *4*, 711–721. [CrossRef]
7. Gaucher, E.C.; Blanc, P. Cement/clay interactions—A review: Experiments, natural analogues, and modeling. *Waste Manag.* **2006**, *26*, 776–788. [CrossRef] [PubMed]
8. Yokoyama, S.; Shimbashi, M.; Minato, D.; Watanabe, Y.; Jenni, A.; Mäder, U. Alteration of bentonite reacted with cementitious materials for 5 and 10 years in the Mont Terri Rock Laboratory (CI Experiment). *Minerals* **2021**, *11*, 251. [CrossRef]
9. Pusch, R. Transport of radionuclides in smectite clay. In *Environmental Interactions of Clays: Clays and the Environment*; Parker, A., Rae, J.E., Eds.; Springer: Berlin/Heidelberg, Germany, 1998; pp. 7–35, ISBN 978-3-662-03651-8.
10. Herbert, H.-J.; Kasbohm, J.; Sprenger, H.; Fernández, A.M.; Reichelt, C. Swelling pressures of MX-80 bentonite in solutions of different ionic strength. *Phys. Chem. Earth Parts A/B/C* **2008**, *33*, S327–S342. [CrossRef]
11. Kaufhold, S.; Dohrmann, R. Stability of bentonites in salt solutions I sodium chloride. *Appl. Clay Sci.* **2009**, *45*, 171–177. [CrossRef]
12. Hofmann, H.; Bauer, A.; Warr, L.N. Behavior of smectite in strong salt brines under conditions relevant to the disposal of low- to medium-grade nuclear waste. *Clays Clay Miner.* **2004**, *52*, 14–24. [CrossRef]
13. Stroes-Gascoyne, S.; Hamon, C.J.; Maak, P. Limits to the use of highly compacted bentonite as a deterrent for microbiologically influenced corrosion in a nuclear fuel waste repository. *Phys. Chem. Earth Parts A/B/C* **2011**, *36*, 1630–1638. [CrossRef]
14. Missana, T.; Alonso, U.; Fernández, A.M.; García-Gutiérrez, M. Colloidal properties of different smectite clays: Significance for the bentonite barrier erosion and radionuclide transport in radioactive waste repositories. *Appl. Geochem.* **2018**, *97*, 157–166. [CrossRef]
15. Meleshyn, A. *Microbial Processes Relevant for Long-Term Performance of Radioactive Waste Repositories in Clays*; GRS-291; GRS: Köln, Germany, 2011.
16. Dong, H.; Jaisi, D.P.; Kim, J.; Zhang, G. Microbe-clay mineral interactions. *Am. Mineral.* **2009**, *94*, 1505–1519. [CrossRef]
17. Muyzer, G.; Stams, A.J.M. The ecology and biotechnology of sulphate-reducing bacteria. *Nat. Rev. Microbiol.* **2008**, *6*, 441–454. [CrossRef]
18. El Mendili, Y.; Abdelouas, A.; Bardeau, J.-F. Insight into the mechanism of carbon steel corrosion under aerobic and anaerobic conditions. *Phys. Chem. Chem. Phys.* **2013**, *15*, 9197–9204. [CrossRef] [PubMed]
19. Pedersen, K.; Bengtsson, A.; Blom, A.; Johansson, L.; Taborowski, T. Mobility and reactivity of sulphide in bentonite clays–Implications for engineered bentonite barriers in geological repositories for radioactive wastes. *Appl. Clay Sci.* **2017**, *146*, 495–502. [CrossRef]
20. Lantenois, S.; Lanson, B.; Muller, F.; Bauer, A.; Jullien, M.; Plançon, A. Experimental study of smectite interaction with metal Fe at low temperature: 1. Smectite destabilization. *Clays Clay Miner.* **2005**, *53*, 597–612. [CrossRef]
21. Soltermann, D. Ferrous Iron Uptake Mechanisms at the Montmorillonite-Water Interface under Anoxic and Electrochemically Reduced Conditions. Ph.D. Thesis, ETH, Zurich, Switzerland, 2014.
22. Ufer, K.; Stanjek, H.; Roth, G.; Dohrmann, R.; Kleeberg, R.; Kaufhold, S. Quantitative phase analysis of bentonites by the Rietveld method. *Clays Clay Miner.* **2008**, *56*, 272–282. [CrossRef]
23. Kaufhold, S.; Stucki, J.W.; Finck, N.; Steininger, R.; Zimina, A.; Dohrmann, R.; Ufer, K.; Pentrák, M.; Pentráková, L. Tetrahedral charge and Fe content in dioctahedral smectites. *Clay Miner.* **2017**, *52*, 51–65. [CrossRef]
24. Wersin, P.; Leupin, O.X.; Mettler, S.; Gaucher, E.C.; Mäder, U.; de Cannière, P.; Vinsot, A.; Gäbler, H.E.; Kunimaro, T.; Kiho, K.; et al. Biogeochemical processes in a clay formation in situ experiment: Part A–Overview, experimental design and water data of an experiment in the Opalinus Clay at the Mont Terri Underground Research Laboratory, Switzerland. *Appl. Geochem.* **2011**, *26*, 931–953. [CrossRef]
25. Meleshyn, A. *Mechanisms of Transformation of Bentonite Barriers (UMB)*; GRS-930; GRS: Köln, Germany, 2019.
26. Matschiavelli, N.; Drozdowski, J.; Kluge, S.; Arnold, T.; Cherkouk, A. Joint project: Umwandlungsmechanismen in Bentonitbarrieren—Subproject B: Einfluss von mikrobiellen Prozessen auf die Bentonitumwandlung, HZDR-103, Dresden, Germany. 2019. Available online: https://www.hzdr.de/db/!Publications?pNid=head&pSelMenu=0&pSelTitle=29398 (accessed on 21 June 2021).
27. Meier, L.P.; Kahr, G. Determination of the Cation Exchange Capacity (CEC) of clay minerals using the complexes of copper (II) Ion with Triethylenetetramine and Tetraethylenepentamine. *Clays Clay Miner.* **1999**, *47*, 386–388. [CrossRef]
28. Stanjek, H.; Künkel, D. CEC determination with Cu-triethylenetetramine: Recommendations for improving reproducibility and accuracy. *Clay Miner.* **2016**, *51*, 1–17. [CrossRef]
29. Doebelin, N.; Kleeberg, R. Profex: A graphical user interface for the Rietveld refinement program BGMN. *J. Appl. Crystallogr.* **2015**, *48*, 1573–1580. [CrossRef]
30. Christidis, G.E. Validity of the structural formula method for layer charge determination of smectites: A re-evaluation of published data. *Appl. Clay Sci.* **2008**, *42*, 1–7. [CrossRef]
31. Williams, D.B.; Carter, C.B. *Transmission Electron Microscopy: A Textbook for Materials Science*, 2nd ed.; Springer: New York, NY, USA; London, UK, 2009; ISBN 978-0-387-76501-3.
32. Velde, B. Electron microprobe analysis of clay minerals. *Clay Miner.* **1984**, *19*, 243–247. [CrossRef]
33. Van der Pluijm, B.A. Analytical electron microscopy and the problem of potassium diffusion1. *Clays Clay Miner.* **1988**, *36*, 498–504. [CrossRef]

34. Newbury, D.E.; Ritchie, N.W.M. Electron-excited X-ray microanalysis by energy dispersive spectrometry at 50: Analytical accuracy, precision, trace sensitivity, and quantitative compositional mapping. *Microsc. Microanal.* **2019**, *25*, 1075–1105. [CrossRef]
35. Stevens, R.E. A system for calculating analyses of micas and related minerals to end members. *US Geol. Surv. Bull.* **1946**, *950*, 101–119.
36. Wolters, F. Classification of Montmorillonites. Ph.D. Thesis, Universität Karlsruhe, Karlsruhe, Germany, 2005.
37. Matschiavelli, N.; Kluge, S.; Podlech, C.; Standhaft, D.; Grathoff, G.; Ikeda-Ohno, A.; Warr, L.N.; Chukharkina, A.; Arnold, T.; Cherkouk, A. The year-long development of microorganisms in uncompacted bavarian bentonite slurries at 30 and 60 °C. *Environ. Sci. Technol.* **2019**, *53*, 10514–10524. [CrossRef]
38. Warr, L.N. IMA-CNMNC approved mineral symbols. *Mineral. Mag.* **2021**, *85*, 291–320. [CrossRef]
39. Moore, D.M.; Reynolds, R.C. *X-ray Diffraction and the Identification and Analysis of Clay Minerals*, 2nd ed.; Oxford University Press: Oxford, UK, 1997; ISBN 978-0-19-508713-0.
40. Emmerich, K.; Wolters, F.; Kahr, G.; Lagaly, G. Clay Profiling: The classification of montmorillonites. *Clays Clay Miner.* **2009**, *57*, 104–114. [CrossRef]
41. Stucki, J.W. A review of the effects of iron redox cycles on smectite properties. *Comptes Rendus Geosci.* **2011**, *343*, 199–209. [CrossRef]
42. Klemps, R.; Cypionka, H.; Widdel, F.; Pfennig, N. Growth with hydrogen, and further physiological characteristics of *Desulfotomaculum* species. *Arch. Microbiol.* **1985**, *143*, 203–208. [CrossRef]
43. Nicholson, W.L.; Munakata, N.; Horneck, G.; Melosh, H.J.; Setlow, P. Resistance of Bacillus endospores to extreme terrestrial and extraterrestrial environments. *Microbiol. Mol. Biol. Rev.* **2000**, *64*, 548–572. [CrossRef] [PubMed]
44. Gauthier, M.J.; Lafay, B.; Christen, R.; Fernandez-Linares, L.C.; Acquaviva, M.; Bonin, P.; Bertrand, J.-C. Marinobacter hydrocarbonoclasticus gen. nov., sp. nov., a new, extremely halotolerant, hydrocarbon-degrading marine bacterium. *Int. J. Syst. Bacteriol.* **1992**, *42*, 568–576. [CrossRef] [PubMed]
45. Pedersen, K. Microbial Processes in Radioactive Waste Disposal, SKB TR-00-04, Stockholm, Sweden. 2000. Available online: https://www.osti.gov/etdeweb/servlets/purl/21330059 (accessed on 14 June 2021).
46. Savage, D. *The Effects of High Salinity Groundwater on the Performance of Clay Barriers*; SKI-R-05-54; Swedish Nuclear Power Inspectorate: Stockholm, Sweden, 2005.
47. Tertre, E.; Prêt, D.; Ferrage, E. Influence of the ionic strength and solid/solution ratio on Ca (II)-for-Na+ exchange on montmorillonite. Part 1: Chemical measurements, thermodynamic modeling and potential implications for trace elements geochemistry. *J. Colloid Interface Sci.* **2011**, *353*, 248–256. [CrossRef] [PubMed]
48. Warr, L.; Berger, J. Hydration of bentonite in natural waters: Application of "confined volume" wet-cell X-ray diffractometry. *Phys. Chem. Earth Parts A/B/C* **2007**, *32*, 247–258. [CrossRef]
49. Christidis, G.E.; Blum, A.E.; Eberl, D.D. Influence of layer charge and charge distribution of smectites on the flow behaviour and swelling of bentonites. *Appl. Clay Sci.* **2006**, *34*, 125–138. [CrossRef]
50. Laird, D.A. Influence of layer charge on swelling of smectites. *Appl. Clay Sci.* **2006**, *34*, 74–87. [CrossRef]
51. Kaufhold, S.; Dohrmann, R.; Koch, D.; Houben, G. The pH of aqueous bentonite suspensions. *Clays Clay Miner.* **2008**, *56*, 338–343. [CrossRef]
52. Beaufort, D.; Berger, G.; Lacharpagne, J.C.; Meunier, A. An experimental alteration of montmorillonite to a di + trioctahedral smectite assemblage at 100 °C and 200 °C. *Clay Miner.* **2001**, *36*, 211–225. [CrossRef]
53. Heller-Kallai, L. Protonation–deprotonation of dioctahedral smectites. *Appl. Clay Sci.* **2001**, *20*, 27–38. [CrossRef]
54. Drits, V.A. A Model for the mechanism of Fe^{3+} to Fe^{2+} reduction in dioctahedral smectites. *Clays Clay Miner.* **2000**, *48*, 185–195. [CrossRef]
55. Rozalen, M.; Huertas, F.J.; Brady, P.V. Experimental study of the effect of pH and temperature on the kinetics of montmorillonite dissolution. *Geochim. Cosmochim. Acta* **2009**, *73*, 3752–3766. [CrossRef]
56. Birgersson, M.; Karnland, O.; Korkeakoski, P.; Sellin, P.; Mäder, U.; Wersin, P. *Montmorillonite Stability Under Near-Field Conditions*; NTB-14-12; National Cooperative for the Disposal of Radioactive Waste (NAGRA): Wettingen, Switzerland, 2014; pp. 1015–2636.
57. Ye, W.-M.; He, Y.; Chen, Y.G.; Chen, B.; Cui, Y.-J. Thermochemical effects on the smectite alteration of GMZ bentonite for deep geological repository. *Environ. Earth Sci.* **2016**, *75*, 906. [CrossRef]
58. Nguyen-Thanh, L.; Herbert, H.-J.; Kasbohm, J.; Hoang-Minh, T.; Mählmann, R.F. Effects of chemical structure on the stability of smectites in short-term alteration experiments. *Clays Clay Miner.* **2014**, *62*, 425–446. [CrossRef]
59. Stroes-Gascoyne, S.; Sergeant, C.; Schippers, A.; Hamon, C.J.; Nèble, S.; Vesvres, M.-H.; Barsotti, V.; Poulain, S.; Le Marrec, C. Biogeochemical processes in a clay formation in situ experiment: Part D–Microbial analyses–Synthesis of results. *Appl. Geochem.* **2011**, *26*, 980–989. [CrossRef]
60. Fru, E.C.; Athar, R. In situ bacterial colonization of compacted bentonite under deep geological high-level radioactive waste repository conditions. *Appl. Microbiol. Biotechnol.* **2008**, *79*, 499–510. [CrossRef] [PubMed]
61. Cai, P.; Huang, Q.; Zhang, X.; Chen, H. Adsorption of DNA on clay minerals and various colloidal particles from an Alfisol. *Soil Biol. Biochem.* **2006**, *38*, 471–476. [CrossRef]
62. Greaves, M.P.; Wilson, M.J. The adsorption of nucleic acids by montmorillonite. *Soil Biol. Biochem.* **1969**, *1*, 317–323. [CrossRef]
63. Hobbie, S.N.; Li, X.; Basen, M.; Stingl, U.; Brune, A. Humic substance-mediated Fe (III) reduction by a fermenting Bacillus strain from the alkaline gut of a humus-feeding scarab beetle larva. *Syst. Appl. Microbiol.* **2012**, *35*, 226–232. [CrossRef]

64. Bai, Y.; Mellage, A.; Cirpka, O.A.; Sun, T.; Angenent, L.T.; Haderlein, S.B.; Kappler, A. AQDS and Redox-Active NOM enables microbial Fe (III)-mineral reduction at cm-scales. *Environ. Sci. Technol.* **2020**, *54*, 4131–4139. [CrossRef] [PubMed]
65. Jaisi, D.P.; Kukkadapu, R.K.; Eberl, D.D.; Dong, H. Control of Fe (III) site occupancy on the rate and extent of microbial reduction of Fe (III) in nontronite. *Geochim. Cosmochim. Acta* **2005**, *69*, 5429–5440. [CrossRef]
66. Pankhania, I.P.; Spormann, A.M.; Hamilton, W.A.; Thauer, R.K. Lactate conversion to acetate, CO_2 and H_2 in cell suspensions of Desulfovibrio vulgaris (Marburg): Indications for the involvement of an energy driven reaction. *Arch. Microbiol.* **1988**, *150*, 26–31. [CrossRef]
67. Thauer, R.K.; Möller-Zinkhan, D.; Spormann, A.M. Biochemistry of acetate catabolism in anaerobic chemotrophic bacteria. *Annu. Rev. Microbiol.* **1989**, *43*, 43–67. [CrossRef]
68. Daniels, L.; Sparling, R.; Sprott, G. The bioenergetics of methanogenesis. *Biochim. Biophys. Acta (BBA)—Rev. Bioenerg.* **1984**, *768*, 113–163. [CrossRef]
69. Courdouan, A.; Christl, I.; Meylan, S.; Wersin, P.; Kretzschmar, R. Isolation and characterization of dissolved organic matter from the Callovo–Oxfordian formation. *Appl. Geochem.* **2007**, *22*, 1537–1548. [CrossRef]
70. Ramos, M.E.; Huertas, F.J. Adsorption of lactate and citrate on montmorillonite in aqueous solutions. *Appl. Clay Sci.* **2014**, *90*, 27–34. [CrossRef]
71. Grigoryan, A.A.; Jalique, D.R.; Medihala, P.; Stroes-Gascoyne, S.; Wolfaardt, G.M.; McKelvie, J.; Korber, D.R. Bacterial diversity and production of sulfide in microcosms containing uncompacted bentonites. *Heliyon* **2018**, *4*, e00722. [CrossRef]